ARL-TR-8918 • MAR 2020

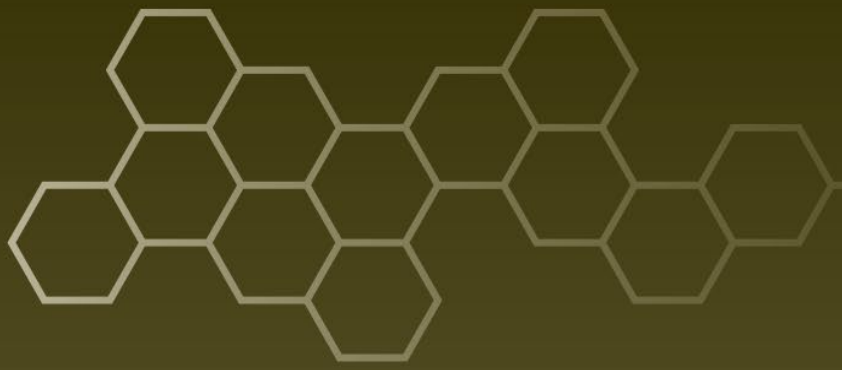

Modeling the Combustion of Opposed Flows of Butadiene and Air: A Skeletal Finite-Rate Chemical Kinetics Mechanism Derived from the San Diego Mechanism and Regression Rate Predictions for Hydroxyl-Terminated Polybutadiene–Air Systems

by Michael McQuaid

NOTICES

Disclaimers

The findings in this report are not to be construed as an official Department of the Army position unless so designated by other authorized documents.

Citation of manufacturer's or trade names does not constitute an official endorsement or approval of the use thereof.

Destroy this report when it is no longer needed. Do not return it to the originator.

ARL-TR-8918 ● MAR 2020

Modeling the Combustion of Opposed Flows of Butadiene and Air: A Skeletal Finite-Rate Chemical Kinetics Mechanism Derived from the San Diego Mechanism and Regression Rate Predictions for Hydroxyl-Terminated Polybutadiene–Air Systems

Michael McQuaid
Weapons and Materials Research Directorate, CCDC Army Research Laboratory

REPORT DOCUMENTATION PAGE

Form Approved
OMB No. 0704-0188

1. REPORT DATE *(DD-MM-YYYY)*	2. REPORT TYPE	3. DATES COVERED (From - To)
March 2020	Technical Report	01 Oct 2019–15 Jan 2020

4. TITLE AND SUBTITLE

Modeling the Combustion of Opposed Flows of Butadiene and Air: A Skeletal Finite-Rate Chemical Kinetics Mechanism Derived from the San Diego Mechanism and Regression Rate Predictions for Hydroxyl-Terminated Polybutadiene–Air Systems

5a. CONTRACT NUMBER

5b. GRANT NUMBER

5c. PROGRAM ELEMENT NUMBER

6. AUTHOR(S)

Michael McQuaid

5d. PROJECT NUMBER

5e. TASK NUMBER

5f. WORK UNIT NUMBER

7. PERFORMING ORGANIZATION NAME(S) AND ADDRESS(ES)

CCDC Army Research Laboratory
ATTN: FCDD-RLW-LD
Aberdeen Proving Ground, MD 21005

8. PERFORMING ORGANIZATION REPORT NUMBER

ARL-TR-8918

9. SPONSORING/MONITORING AGENCY NAME(S) AND ADDRESS(ES)

10. SPONSOR/MONITOR'S ACRONYM(S)

11. SPONSOR/MONITOR'S REPORT NUMBER(S)

12. DISTRIBUTION/AVAILABILITY STATEMENT

Approved for public release; distribution is unlimited.

13. SUPPLEMENTARY NOTES

ORCID ID: Michael McQuaid, 0000-0001-5523-7468

14. ABSTRACT

To evaluate the potential of a homogeneous-reactor (HR)-simulation-based implementation of the trial mechanism method (TMM) to produce skeletal finite-rate chemical kinetics mechanisms that are valid for modeling solid-fuel ramjet (SFRJ) combustor dynamics, one was employed to reduce the San Diego (SD) mechanism to produce candidates for modeling opposed-flow burner experiments involving hydroxyl-terminated polybutadiene (HTPB) and N_2–O_2 mixtures. A candidate with 63 reactions and 33 species was vetted for the application. It was confirmed that when it was substituted for the (full) SD mechanism in HR simulations with initial conditions similar to those expected to be realized near HTPB's pyrolyzing surface, temperature and rate of heat release versus time histories produced with the full mechanism were reasonably reproduced. In addition, when it was substituted for the full mechanism in relevant opposed-flow diffusion flame simulations, key features, including the temperature gradient adjacent to the fuel inlet, the system's maximum temperature, and that temperature's location, were reasonably reproduced. In addition, HTPB regression rate predictions produced with the full mechanism and with the candidate were in reasonable agreement. The evaluation thus indicated that an HR-simulation-based TMM implementation can produce skeletal mechanisms that are valid for modeling SFRJ combustor dynamics.

15. SUBJECT TERMS

thermochemical kinetics, solid fuel ramjet, combustion, deflagration modeling, rocket propulsion

16. SECURITY CLASSIFICATION OF:			17. LIMITATION OF ABSTRACT	18. NUMBER OF PAGES	19a. NAME OF RESPONSIBLE PERSON
a. REPORT	b. ABSTRACT	c. THIS PAGE			Michael McQuaid
Unclassified	Unclassified	Unclassified	UU	52	19b. TELEPHONE NUMBER (Include area code) (410) 278-6185

Contents

List of Figures

List of Tables

1. Introduction

The combustion of 1,3-butadiene (C_4H_6) has been extensively investigated. A Web of Science search prompted by the topic "butadiene and combustion" returned citations for 515 potentially relevant studies. The motivations for them were manifold. Seeking through modeling insights into the processes that underlie the performance and sensitivity of composite rocket propellants and explosives, Department of Defense-sponsored researchers have investigated the topic because hydroxyl-terminated polybutadiene (HTPB) is widely employed as a binder in such formulations and C_4H_6 is thought to be a reasonable surrogate for the product(s) of HTPB's pyrolysis (Beckstead et al. 2007). HTPB has also been used in neat form and as a binder for fuel grains in solid-fuel ramjets (SFRJs) (McDonald et al. 2017), and its combustion in that application motivated the study summarized here. SFRJs are air-breathing engines in which the compression of air that is needed to raise its temperature and pressure to values at which a fuel–air mixture will efficiently combust is provided by the projectile's forward motion (alone). Offering a good balance of (mechanical) simplicity, (relatively) low cost, specific impulse, and speed, an SFRJ also will not respond violently to threats of concern, making it an insensitive munitions technology as well.

Despite the many positive attributes of the SFRJ concept, the technical challenges that must be overcome to realize them are considerable. Ignition and the maintenance of flame/combustion stability throughout flight are prominent design issues. Ignition is difficult because air speeds approaching Mach 2 are required to produce the compression of air needed for combustion to be sustained. In addition, because compression is due solely to the forward motion of the projectile, the orientation of the projectile with respect to that motion can greatly impact the combustion process. Projectiles need to be (gradually) "banked" rather than (sharply) "skidded" into turns to reduce the risk of the engine flaming out.

To predict an SFRJ's performance over wide ranges of potentially relevant flight scenarios, knowledge of flame holding requirements, fuel regression rate as a function of flight speed and altitude, and diffusion-controlled combustion is required (Krishnan and George 1998). However, all these phenomena are driven by thermochemical (reaction) kinetics, and the mechanisms that have been developed to represent them in SFRJ combustor models have tended to be simplified, semi-empirical constructs (Gariani et al. 2011; Kumar and Kumar 2013; Sun et al. 2015; Morinigo and Hermida-Quesada 2016). Therefore, their range of validity is uncertain, making the models' predictions for engine performance at "off-design" (but potentially relevant) conditions similarly uncertain.

To address this issue, researchers at the US Army Combat Capabilities Development Command (CCDC) Army Research Laboratory (ARL), Naval Research Laboratory, Naval Air Warfare Center, and Naval Sea Warfare Center have proposed a collaborative effort designed to elucidate the mechanisms of HTPB–air combustion in SFRJ combustors. In the proposed effort, flames produced by combusting (solid) HTPB and (gaseous) N_2–O_2 mixtures in an opposed-flow burner will be probed with various spectroscopic techniques, and those experiments will be modeled. ARL researchers will be responsible for developing detailed finite-rate chemical kinetics mechanisms to represent the gas phase's thermochemical kinetics.

Regarding that aspect of the effort, Chen and McQuaid (2009, 2010, 2011, 2015, 2020) have assembled a comprehensive mechanism for modeling the ignition and combustion HTPB pyrolysis products mixed with air that includes elementary reactions for decomposing a relatively large hydrocarbon ($C_{20}H_{32}$) with attributes similar to HTPB type R45M polymer chains. However, there was interest in employing a general, open-source chemical kinetics mechanism for modeling hydrocarbon–air combustion that was developed by the University of California San Diego Combustion Research Group. Called by its developers "the San Diego (SD) mechanism", when the effort summarized here commenced, it comprised five separate modules and a mechanism suitable for modeling the combustion of C_4H_6–air mixtures could be constructed by combining three of them. With (exact) duplicate reactions eliminated, the combination comprised inputs for computing rates for 323 elementary reactions and thermochemical and transport properties for 67 species.

Unlike ARL's $C_{20}H_{32}$–air mechanism, which (at present) comprises more than 2750 reactions and more than 800 species (McQuaid and Chen 2020), the full (323 reaction-67 species) SD mechanism is a practical option for steady laminar quasi-1-D opposed-flow diffusion flame (OFDF) models that have the potential to reasonably simulate the proposed experiments. Those models' ability to reproduce results derived from the experiments will therefore constitute a basis for justifying the SD mechanism's employment for multidimensional, temporally transient computational fluid dynamics (CFD) SFRJ combustor models. However, scaling quadratically to cubically with the numbers of reactions and species in the chemical kinetics mechanism, the computational costs of SFRJ combustor simulations are considerably higher than those of steady 1-D OFDF simulations, and therefore impose much more restrictive limits on the sizes of the mechanisms that can be used. For example, the limits for a mechanism that can be used by an SFRJ combustor model being developed at ARL are about 120

reactions and 100 species (Nusca et al. 2019; Chen and McQuaid 2020). Therefore, the SD mechanism is too large for that application.

To address such issues, ARL has developed and applied implementations of the trial mechanism method (TMM) to create skeletal/reduced mechanisms that will mimic a full mechanism within a delimited parameter space (Kotlar 2010; McQuaid 2013). The TMM (concept) predicates the elimination of reactions from a full one based on comparisons of full- and trial-mechanism-based solutions for combustion problems that are relevant to, but (significantly) less expensive to solve than, those of specific interest. To date, the time evolution of a homogeneous reacting gas mixture is the only combustion problem type that ARL has employed for this purpose. (Considered "canonical", problems of this type will also be referred to herein as homogeneous reactor [HR] simulations.) Applied to reduce mechanisms for a wide variety of applications (Kotlar 2010; McQuaid 2013; Chen and McQuaid 2016; McQuaid et al. 2019), TMM implementations based on analyzing the solutions to HR problems have been found to work well (with respect to reducing mechanisms to targeted sizes), and I have yet to see results produced by the CFD models that employ a TMM-produced skeletal mechanism that raise questions about the mechanism's validity. But that observation requires qualification. In most cases, the validation was simply that the CFD model was able to reproduce (measured) global parameters, such as chamber pressure, thrust, and/or burning rates. Although such validations are important and encouraging, given the complexity of the dynamics in such simulations and the vagaries of CFD modeling—the use of a skeletal mechanism in a CFD model tacitly admits that one simply needs one that is "good enough"—it can be very difficult to ascertain whether "significant" shortcomings of the skeletal mechanisms were not revealed because they were masked or compensated for by other (modeled) processes.

That said, there is reason to expect that an HR-simulation-based implementation of the TMM will produce candidates that will mimic well a full mechanism's ability to represent the thermochemical kinetics associated with the ignition and combustion of monopropellants and explosives. Evolving with distance from the burning surface of such materials, a (starting) chemical composition (and the concomitant energy release) in a steady flame is likely to be mirrored by the temporal evolution of that same chemical composition in an HR simulation. (Indeed, the spatial dimension of a steady 1-D flame can be transformed into a temporal domain (τ) via $\tau(x) = \int_0^x \left[v_g(x')\right]^{-1} dx'$, where v_g is the velocity of the gas.) A compelling example of such mirroring is observed when comparing HR and premixed-1-D-flame simulations involving nitrate esters and/or nitramines. Flames produced by the combustion of these material classes exhibit a two-stage

structure that reflects well-defined exothermic transients separated in x (or τ), and analogous transients separated in time (t) occur in HR simulations.

The potential for an HR-simulation-based TMM implementation to produce a skeletal mechanism that will mimic well a full one's ability to represent the thermochemical kinetics associated with the combustion of a solid fuel (grain) and a gaseous or liquid oxidizer is more speculative. Adjacent to the solid–gas (or liquid) interface, the fuel and oxidizer (components) are not well mixed, and it cannot be expected that the spatial/temporal evolution of the chemical composition will be mirrored in an HR simulation.

Concerned about this issue, I thought a reduction of the SD mechanism might prove instructive. Because it is small enough to be employed as the thermochemical kinetics basis for a quasi-1-D steady laminar OFDF model with the potential to reasonably simulate the proposed experiments, it can be used to predict the regression rates that will be measured in those experiments, and predictions produced by reduced mechanisms can be compared to them. Moreover, the proposed experiments should generate data such as species and temperature profiles that will facilitate more critical evaluations of a skeletal mechanism's ability to mimic the SD mechanism within the parameter space expected to be realized in the experiments.

A relatively straightforward application of an HR-simulation-based TMM implementation produced a reasonably large number of fairly small mechanisms, and the capacity of a candidate with 63 reactions and 33 species to mimic the SD mechanism within the prescribed parameter space was vetted. I confirmed that when it was employed as the (thermochemical-kinetics) basis for HR simulations whose results were screened to determine whether or not a reaction could be eliminated, it produced temperature (T) and rate of heat release ($\dot{q}$) versus time (t) histories that were in reasonable agreement with those produced with the SD mechanism. In addition, when it was employed as the basis for simulating relevant OFDFs, key features of solutions produced with the SD mechanism were well reproduced.

The OFDF simulations were also the basis for predicting HTPB's regression rate as a function of pressure and the velocity of a flow of air assuming the temperature of HTPB's burning surface was either 500 or 650 K. The model for predicting regression rates was based on the CYCLOPS framework (Miller and Anderson 2000, 2004). Derived from general equations for representing energy, mass, and species conservation at a planar condensed-phase–gas-phase interface, it is predicated on the assumption that all condensed-phase processes (including reaction kinetics, phase changes, and diffusion) can be neglected. Miller and

Anderson developed and employed the framework because they did not consider the then-current knowledge of condensed-phase processes sufficient to develop reliable representations for them, and they doubted those circumstances were likely to be remedied in the (then) near future. In general, that is still the case today.

Its relative simplicity notwithstanding, the CYCLOPS framework has been successfully employed to predict the burning rates of various monopropellants and explosives (Miller and Anderson 2000, 2004; McQuaid and Chen 2014; Chen at al. 2019). Indeed, reducing the calculation of burning/regression rate predictions to their most basic/necessary (and well-founded) elements, it facilitates focusing on those elements and quantifying their importance (McQuaid and Chen 2014; Chen et al. 2019). Moreover, if it can be shown that reasonable predictions can be obtained absent submodels for nebulous properties and processes, then the development of simpler, less computationally demanding CFD combustor models can be justified. Thus, I thought predictions based on the CYCLOPS framework would well serve this investigation.

The regression rate predictions produced with the SD mechanism appeared to be reasonable, and predictions produced with the skeletal mechanism well reproduced them. As such, the study indicated an HR-simulation-based TMM implementation can produce skeletal mechanisms for representing the thermochemical kinetics associated with SFRJ combustor dynamics that have validities similar to the mechanism from which they are derived. For reference, the skeletal mechanism's species, reactions, and reaction rate-coefficient parameterizations are provided.

2. Overview of the San Diego Mechanism

The SD mechanism was downloaded from a website maintained by the developers (https://web.eng.ucsd.edu/mae/groups/combustion/mechanism.html). Per the website, "it was derived by beginning with simple chemical systems then proceeding gradually to more complex systems". A mechanism suitable for modeling C_4H_6-O_2 combustion was assembled by combining CK 2016-12-14, CK 2002-10-01 (for JP-10 chemistry), CK 2015-03-01 (for heptane chemistry), and the thermodynamic and transport property data associated with them. The (raw) assembly comprised 335 reactions and 67 species. However, some of the reactions

were "exact" (as opposed to "declared") duplicates. With the exact duplicates eliminated, the mechanism had only 323 reactions.*

3. Computational Methods

3.1 The Trial Mechanism Method

More complete descriptions of the TMM are given elsewhere (Kotlar 2010; McQuaid 2013a). The steps performed for the reductions reported here included the following:

- Creating a set of SD mechanisms with random reaction orderings.
- Sequentially eliminating (single) reactions from each ordering on a trial basis.
- For each elimination, solving HR problems based on the trial mechanism created by the elimination.
- Permanently eliminating the reaction if changes in the values of selected parameters of the solutions produced with the trial mechanism deviated less than specified amounts from standards produced with the full mechanism.

A species was eliminated as a consequence of all reactions involving it being eliminated.

*Occurrences of duplicates were identified by the "mechanism interpreter" employed to convert the downloaded files into the inputs utilized (directly) by the HR and OFDF models. However, the interpreter did not (completely) recognize the equivalence between

2C2H3<=>C4H6	1.26E+13	0.0	0.0	(R1)

and

C4H6 =>2C2H3	1.80E+13	0.0	85126.7	(R1a)
2C2H3 =>C4H6	1.26E+13	0.0	0.0	(R1b)

It flagged R1 and R1a as duplicates. However, observing the difference in the constants prescribing their rate-coefficients, I thought they corresponded to different paths. Therefore I "declared" them, and the (full) mechanism that was reduced, included all three. Since none of these reactions were in the skeletal mechanism that was selected for further vetting, additional reductions were not performed after the equivalence of R1 and R1a–R1b was recognized. All simulations subsequently performed with the SD mechanism did not include R1a or R1b, and only results derived from those simulations are presented in this report.

The program employed to formulate and solve the HR problems was derived from pre-commercial CHEMKIN subroutine libraries (Kee et al. 2002). Their differential-algebraic equation systems were solved with DASPK (Li and Petzold 1999). Stone (2020) refactored a number of subroutines in the two libraries, enabling them to exploit OpenMP parallelism, and thereby reduce simulation run times.

As in prior reductions performed by Kotlar (2010) and me (McQuaid 2013a; Chen and McQuaid 2016; McQuaid et al. 2019; Chen and McQuaid 2020), the parameters of the solutions whose values were compared were local maxima in the mass-specific and volumetric rate of heat release ($\dot{q}_{mass}^{max}$ and $\dot{q}_{vol}^{max}$, respectively) versus t histories, the times at which those maxima occurred (t_{mass}^{max} and t_{vol}^{max}, respectively), and the temperature at the end of the simulation (T_{final}). The rationale for comparing the values of these (and only these) parameters has been discussed previously (McQuaid 2013b). The values of $\dot{q}_{vol}$ and $\dot{q}_{mass}$ at a given t were calculated per

$$\dot{q}_{mass} = R\left(T\sum_k^K \frac{dY_k}{dt}/W_k + \frac{dT}{dt}\sum_k^K Y_k/W_k\right) \tag{1}$$

and

$$\dot{q}_{vol} = \rho_g * \dot{q}_{mass} \tag{2}$$

respectively, where R is the universal gas constant, and for a mechanism with K species, Y_k is the mass fraction of the k^{th} species, W_k is its molecular weight, and ρ_g is the gas-mixture's density.

The initial conditions for the HR problems were chosen based on expectations for the conditions that will be found in the planned OFDF experiments. Provided by Dr Brian Bojko (2019), they were the following: pressures (P) that ranged from 0.3 to 6.2 atm, (mass-based) oxidizer-to-fuel ratios (O/Fs) that ranged from 5 to 40, and temperatures near the burning surface that ranged from 500 to 650 K.

Compared to most mechanisms I have reduced for use in CFD models (McQuaid 2013a; Chen and McQuaid 2016; McQuaid et al. 2019; Chen and McQuaid 2020), the SD mechanism is relatively small, and the central processing unit wall times for HR simulations based on them were extremely short (i.e., generally less than 1 s). In addition, the prescribed parameter space over which the skeletal mechanism was required to mimic the SD mechanism was relatively small. Consequently, the reduction protocol could have included tens of simulations, which, formulated such that conditions throughout the parameter space of interest (including its bounds)

were represented, would have increased the probability that the candidates would well mimic the SD mechanism over the space's entirety. However, I was more interested in evaluating how the method performed when implemented based on the types of compromises that are required for more challenging cases, and approached the development of the protocol as I would for them.

Because the pressure is constant across the spatial domain of an OFDF (simulation) and there were no plans for using an external heat source to promote combustion in the experiments, the HR problems were formulated such that their solutions simulated adiabatic constant pressure processes. Moreover, because the prescribed pressure range was relatively small (0.3–6.2 atm), I assumed it would be sufficient to perform all the simulations at the same pressure, and selected 1 atm, which is near the prescribed range's logarithmic mean (1.4 atm). Similarly, I did not think it was necessary for the problem set to comprise O/F cases that completely spanned 5 to 40, and specified one each at 7.5, 15, and 30. In establishing the chemical compositions that corresponded to these O/Fs, I assumed "air" was 78 mol% N_2, 21 mol% O_2, and 1 mol% Ar. The "fuel" was 100 mol% C_4H_6. An O/F equal to 15 was nearly stoichiometric to CO_2 and H_2O (i.e., a fuel-air equivalence ratio (ϕ) near 1).

The selection of the starting temperature(s) for the HR simulations was not as straightforward. I assumed the time scales of the dynamics in the planned OFDF experiments would be less than 1 s. However, "ignition delays" in the HR simulations (viz. time to the first [and only] significant $\dot{q}_{mass}^{max}/\dot{q}_{vol}^{max}$) were greater than 2.8×10^4 s (2 days) when the starting temperature was at the upper limit of the prescribed range (650 K). With the starting temperature specified to be 750 K, the ignition delays were found to be of $O(10^2$ s). Though still longer than I was completely comfortable with, I was also uncomfortable with further increasing the starting temperature, and therefore settled on 750 K as a reasonable compromise between the competing considerations. STANJAN (Reynolds 1986) was employed to calculate the adiabatic flame temperature (T_{ad}) for each set of initial conditions.

Table 1 shows the initial conditions of the HR problems whose solutions were analyzed. A total of 40 different orderings of the SD mechanism's reactions were processed. For the first pass through an ordering, the maximum acceptable deviations (MADs) from standards for $\dot{q}_{mass}^{max}$, $\dot{q}_{vol}^{max}$, t_{mass}^{max}, and t_{vol}^{max} were set at ±1%, and the MADs in T_{final} were set at ±1 K. Those MADs were subsequently (and collectively) relaxed in ±1% and ±1 K increments, respectively. The largest MADs allowed were ±10% and ±10 K.

Table 1. Initial conditions of HR simulations employed for TMM-based reductions

Set	Started	Completed	Sim.	O/F	ϕ	Initial temp. (K)	Pressure (atm)	Sim. length (s)
A	40	40	1	15	1.08	750	1.0	500
			2	7.5	2.16	750	1.0	300
			3	30	0.54	750	1.0	750

3.2 Opposed-Flow Diffusion Flame Simulations

A slightly modified version of the (pre-commercial) CHEMKIN-III program OPPDIF (Lutz et al. 1997; Stone 2020) was employed to formulate and solve steady laminar quasi-1-D OFDF problems whose solutions were expected to resemble the planned experiments. Consideration of an OFDF-based study of 1,3-butadiene–O_2 combustion by Moshammer et al. (2017) was helpful in getting started. It provided guidance with respect to specifying the separation between the fuel and oxidizer inlets (1.25 cm), the velocities of the gases at the fuel (V_{fuel}) and oxidizer (V_{ox}) inlets (10's of centimeters per second and of similar magnitude), the mass fraction of C_4H_6 in the efflux from the fuel inlet, and the temperature profile to expect for the specified C_4H_6:O_2 ratio ($\phi >> 1$). Once that problem was solved, a succession of problems with initial estimates for state variables derived from the solution to the previous one were solved, facilitating the generation of OFDF simulations with characteristics similar to those that are expected to be realized in the proposed experiments. A representative input deck showing specifications for parameters common to all the OFDF simulations discussed herein is provided in Appendix A. The value of $\dot{q}_{mass}$ at each grid point (j) was computed per

$$\dot{q}_{mass} = -\sum_k^K \dot{\omega}_k \, h_g^k / \rho_g, \tag{3}$$

where $\dot{\omega}_k$ is species k's molar conversion rate and h_g^k is its molar enthalpy. The first grid point ($j = 1$) corresponded to the fuel inlet ($x = 0$ cm).

3.3 Regression Rate Predictions

Predictions for HTPB's regression rate as a function of P, V_{ox}, and T_{fuel} values expected to be realized in the proposed experiments were calculated based on a slight variation of the CYCLOPS framework (Miller and Anderson 2000, 2004). As mentioned in the introduction, that framework was devised to predict the burning rates of monopropellants and explosives, and follows from the assumption that chemical reactions and diffusion in the condensed phase can be neglected. When valid, the 1-D energy-flux-boundary condition at the condensed-phase–gas-phase interface ($x = 0$) reduces to

$$\left[\lambda_g \frac{dT}{dx}\right]^{+0} = r\rho_c\left(\sum_k^K (Y_g^k)^{-0}(h_g^k)^{+0} - h_c^{-\infty}\right) \quad (4)$$

where the left-hand side of the equation corresponds to the energy flux incident on the interface due to the thermal conductivity (λ_g) and the temperature gradient (dT/dx) adjacent to the gas-phase side of the interface ($x = +0$), and the right-hand side corresponds to the energy flux needed to raise the enthalpy of a mass flux with density ρ_c from the value for the condensed phase at $x = -\infty$ ($h_c^{-\infty}$) to that of a set of nascent gas-phase products with mass fractions Y_g^k and enthalpies h_g^k. The parameters λ_g, $\frac{dT}{dx}$, and the h_g^k depend on the temperature of the interface (T^0); λ_g and dT/dx also depend on the pressure.

Since monopropellants and explosives (in effect) comprise both the fuel and oxidizer of a combustible mixture, the prediction of their burning rates via the CYCLOPS framework involves employing a steady laminar burner-stabilized 1-D premixed flame model to simulate the gas-phase processes associated with such materials' deflagrations, and the inlet (viz. the first grid point ($j = 1$)) corresponds to the interface between the condensed and gas phases. Not valid for predicting HTPB's regression rate when it is exposed to a flow of air, the 1-D premixed flame model was replaced with OPPDIF for this study. In this variation, the fuel inlet corresponds the interface between the condensed and gas phases. OPDIFF predicates the fuel entering at $x = 0$. Therefore, the temperature at the fuel inlet (T_{fuel}) corresponds to T^0.

Further assuming that the only gas-phase product of HTPB's pyrolysis was C_4H_6, $[(Y_g^{C_4H_6})^{-0} = 1]$, the energy-flux-boundary condition was

$$\left[\lambda_g \frac{dT}{dx}\right]^{+0} = r\rho_c\left[(h_g^{C_4H_6})^{+0} - h_c^{-\infty}\right]. \quad (5)$$

To complete the calculation, HTPB's ρ_c and $h_c^{-\infty}$ had to be specified. For ρ_c, a fairly narrow range of values was found in links returned by a Google-based search, and I selected 0.9 g/cm^3 (Shark et al. 2014). The specification of $h_c^{-\infty}$'s value was less straightforward. An extremely wide range was found. The value specified (-40 cal/g) represented a nominal value near the middle of several from sources I was familiar with and trusted.

I assumed Eq. 5 was satisfied when

$$\left|\frac{r\rho_c\left[(h_g^{C_4H_6})^{+0} - h_c^{-\infty}\right]}{\left[\lambda_g \frac{dT}{dx}\right]^{+0}} - 1\right| \leq 0.01. \quad (6)$$

This criterion was considered sufficient for the purposes of this study because for a given/fixed combination of P, V_{ox}, and T_{fuel}, the left-hand side of Eq. 6 changed monotonically and with the same order of magnitude (percentage-wise) as changes in V_{fuel}'s value when the right- and left-hand sides of Eq. 5 were within a factor of 10 of one another. Given that mass conservation requires $r\rho_c = V_f\rho_g$ (or $r = V_f\rho_g/\rho_c$), the calculated r were expected to be within 1% of the values that would be obtained if Eq. 5 was satisfied "exactly". Since in general I consider a predicted regression rate to be in good agreement with a measured rate if the two are within a factor of 2 of one another, this criterion was more than sufficient to exclude this consideration as a significant factor in any difference that exceeded a factor of 2.

4. Results

4.1 Candidate Generation

Corresponding to the three HR simulations listed in Table 1, Figs. 1–3 show the T and $\dot{q}_{mass}$ versus t histories analyzed by the TMM's screening algorithm. The histories were relatively simple; in each case, there was only one significant $\dot{q}_{mass}^{max}/\dot{q}_{vol}^{max}$, the temperature rose abruptly to a value near T_{final} when it occurred, and T_{final} was near T_{ad}. I was surprised that the shortest ignition delay was observed in simulation 2. I expected it would be observed in the system that released the most energy per gram of mixture, and therefore would correspond to the system with ϕ closest to 1 (i.e., simulation 1). That system did have the highest T_{ad} and (not surprisingly) produced the highest T_{final}. But that did not result in a shorter ignition delay. Rather, the observed trend called to mind that carbureted internal combustion engines are often "choked" (i.e., run fuel rich) to facilitate their startup. Therefore, it could be rationalized. (Deeper analysis will be required to understand the trend at a mechanistic level.)

The reductions of all 40 orderings proceeded quickly and efficiently, and each produced a candidate with fewer than 80 reactions and fewer than 37 species. An interesting result was that no reactions were eliminated from any ordering when the MADs were ±10% and ±10 K. (I did not attempt to ascertain why.) The smallest candidate comprised 63 reactions and 33 species, and it was selected for further vetting. It is referred to hereafter as A38.09_04. ("A38" is an initial reaction ordering designator. The "09" indicates the MAD level at which it was produced, and the "04" indicates the number of complete passes through the ordering at that level that preceded its creation.) A38.09_04's species, reactions, and reaction rate-coefficient parameterizations are provided in Appendix B.

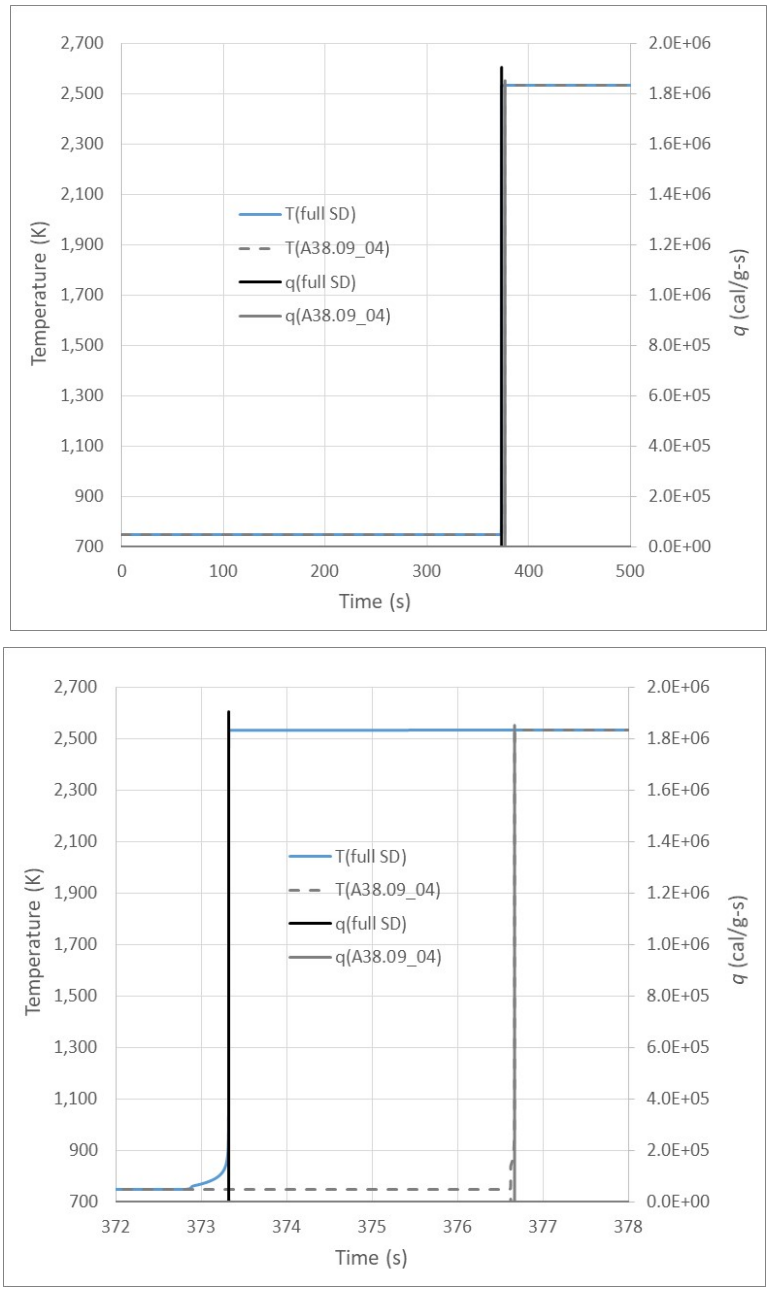

Fig. 1 HR simulation 1: Comparison of results produced with the SD mechanism and with A38.09_04

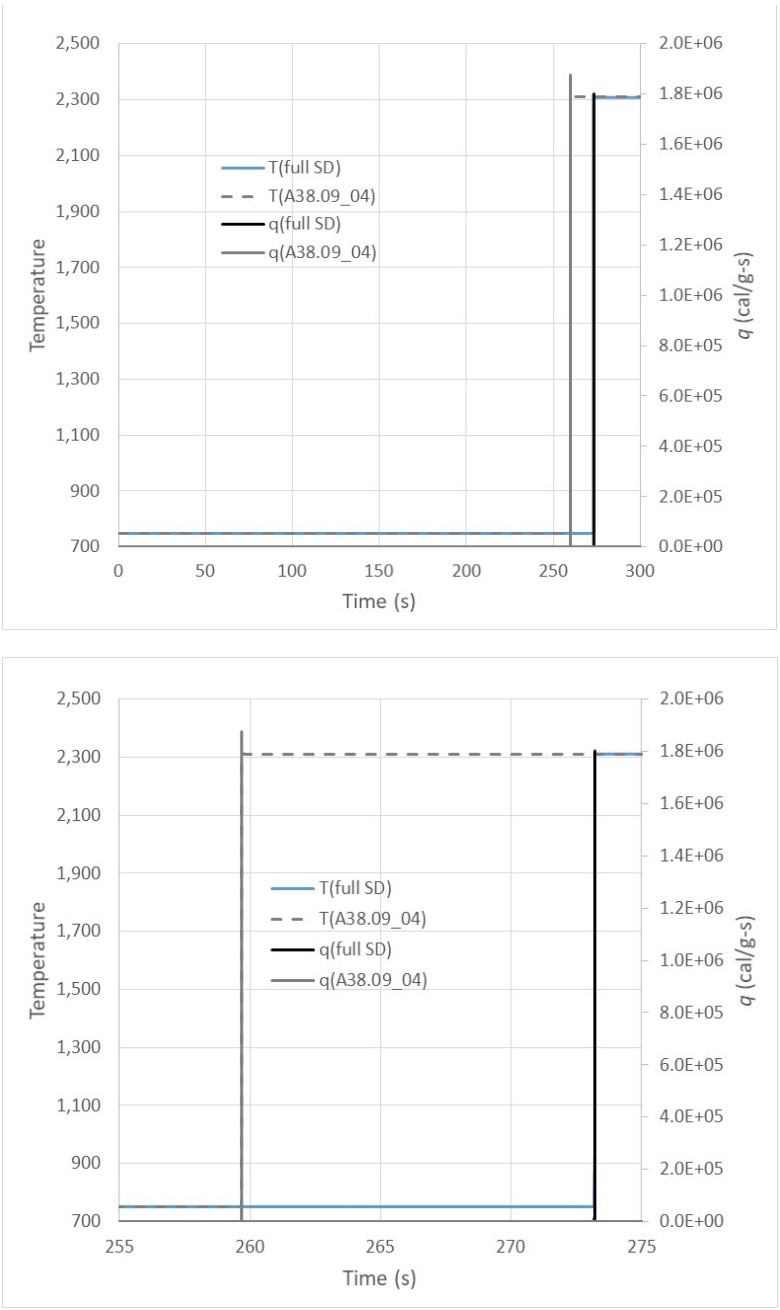

Fig. 2 HR simulation 2: Comparison of results produced with the SD mechanism and with A38.09_04

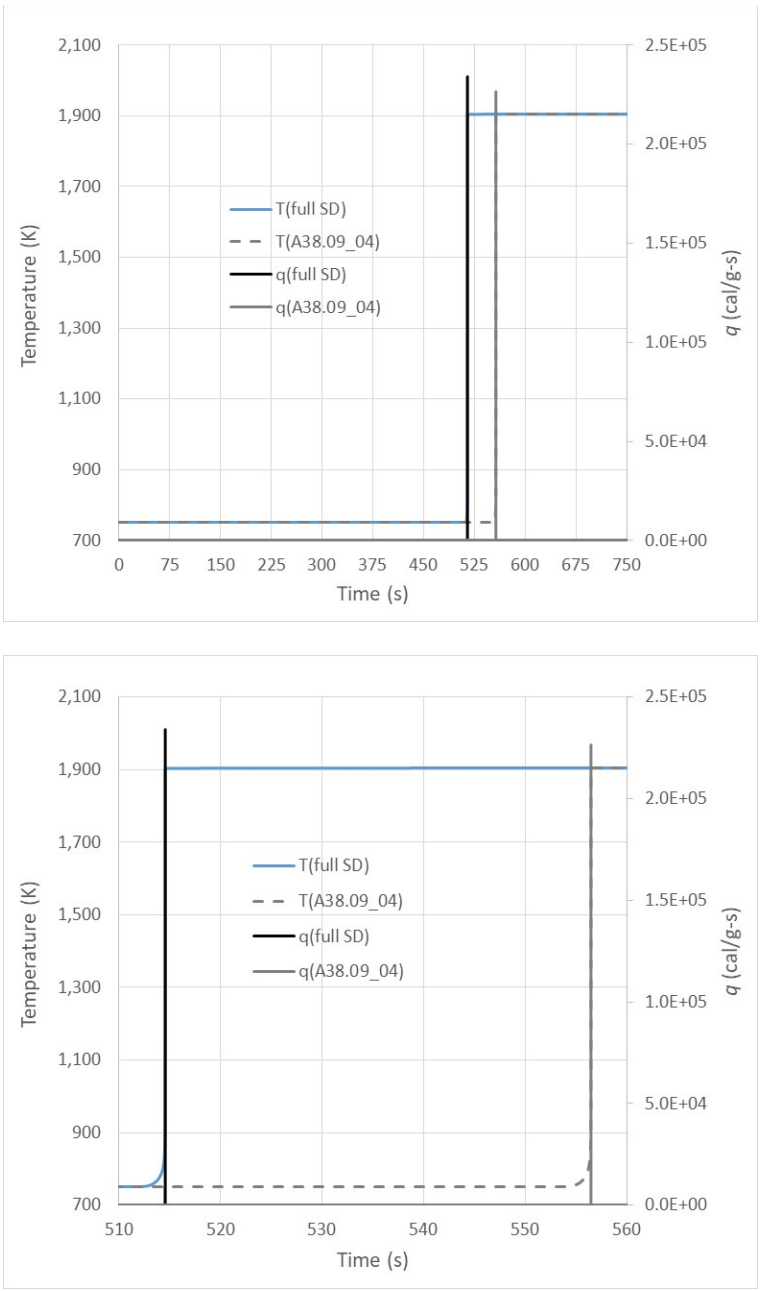

Fig. 3 HR simulation 3: Comparison of results produced with the SD mechanism and with A38.09_04

4.2 Post-Reduction Analyses

4.2.1 Homogeneous Reactor Simulations

Because the algorithm employed to analyze the T and $\dot{q}_{mass}$ versus t histories obtained from the HR simulations was not foolproof, the first step of the validation effort was to compare in their entirety the SD- and A38.09_04-based histories for the three simulations that were the basis for the reduction. As shown in Figs. 1–3, the comparisons confirmed that 1) the histories produced with the two mechanisms were qualitatively similar, 2) the $\dot{q}_{mass}^{max}$ and t_{mass}^{max} values produced with A38.09_04 did not deviate more than ±9% from their corresponding SD-based standard, and 3) the A38.09_04-based T_{final} values did not deviate more than ±9 K from their corresponding SD-based standard.

4.2.2 Opposed-Flow Diffusion Flame Simulations

To predict results that will be measured in the planned experiments, solutions were sought to steady laminar quasi-1-D OFDF problems over the entire ranges of pressure (0.3–6.2 atm), fuel-inlet/burning-surface temperature (500–650 K), and O/F (5–40) anticipated by Bojko (2019). However, in an attempt to solve a problem in which the pressure was 0.3 atm and T_{fuel} was 500 K, the only solution produced (with the resources I was willing to invest) was the "trivial" one (i.e., the temperature decreased monotonically from x = 0 to 1.25 cm). Therefore, I focused instead on obtaining solutions for systems at 0.4 atm, where this issue proved less problematic.

Plots of T and $\dot{q}_{mass}$ versus distance obtained from solutions to 18 different OFDF problems were constructed and inspected. The problems were distinguished by their combination of P, V_{ox}, and T_{fuel} values. (Established via a search to satisfy Eq. 6, V_{fuel}'s value followed from them.) At each of three pressures (0.4, 1.0, and 6.2 atm), three values of V_{ox} were specified that would yield O/Fs across the prescribed range. (The actual O/F could not be firmly established until the V_{fuel} that produced a solution satisfying Eq. 6 was found.) For each of the 9 P-V_{ox} combinations, two problems were formulated and solved: one with T_{fuel} equal to 500 K and the other with it equal to 650 K. For each such pair, the T and $\dot{q}_{mass}$ versus distance plots produced when T_{fuel} was equal to 500 K and when it was equal to 650 K were very similar. Anticipated because the solution at one T_{fuel} was readily obtained by bootstrapping from the other via restart files, they were difficult to distinguish absent y-axis labels. Therefore, only plots derived from problems in which T_{fuel} was 500 K are presented in this report. (Plots for the four T_{fuel} = 500 K cases not presented in this section are presented in Appendix C.)

Plots of T and $\dot{q}_{mass}$ versus distance obtained from solutions to problems for systems at 1 atm and having (overall) O/Fs corresponding to 6.6, 18.1, and 34.6 are shown in Figs. 4–6, respectively. The general features of the $\dot{q}_{mass}$ versus distance plots observed in Figs. 4–6 were also observed in two of the three plots obtained from simulations in which the pressure was 0.4 atm. (The exception is presented and discussed below.) Given the single significant exothermic transient in the corresponding HR simulation, the appearance of two significant $\dot{q}_{mass}^{max}$ as well as an endothermic transient that produced a local $\dot{q}_{mass}$ minimum ($\dot{q}_{mass}^{min}$) was unexpected.

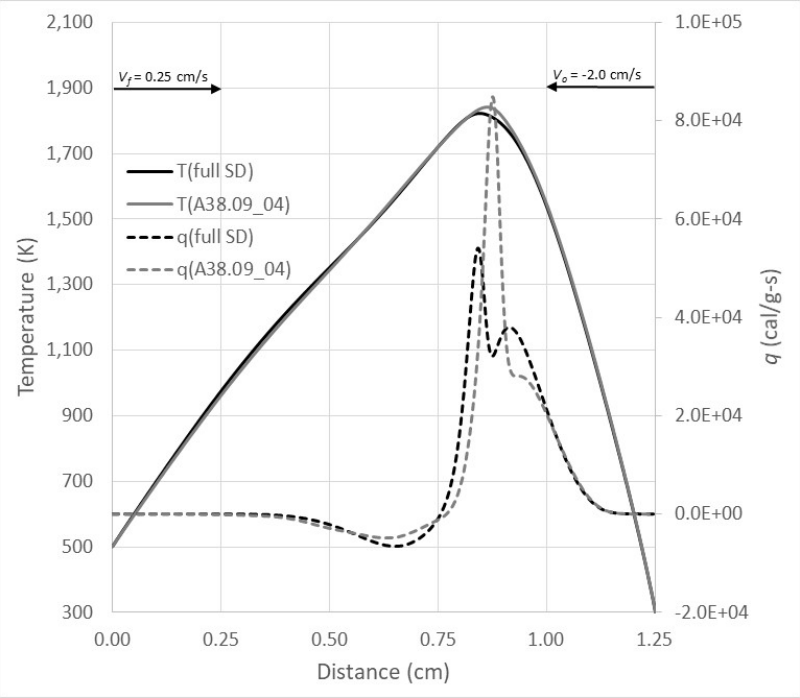

Fig. 4 Comparison of T and $\dot{q}_{mass}$ vs. distance plots obtained from SD- and A38.09_04-based OFDF solutions: P = 1.0 atm, O/F = 6.6, T_{fuel} = 500 K

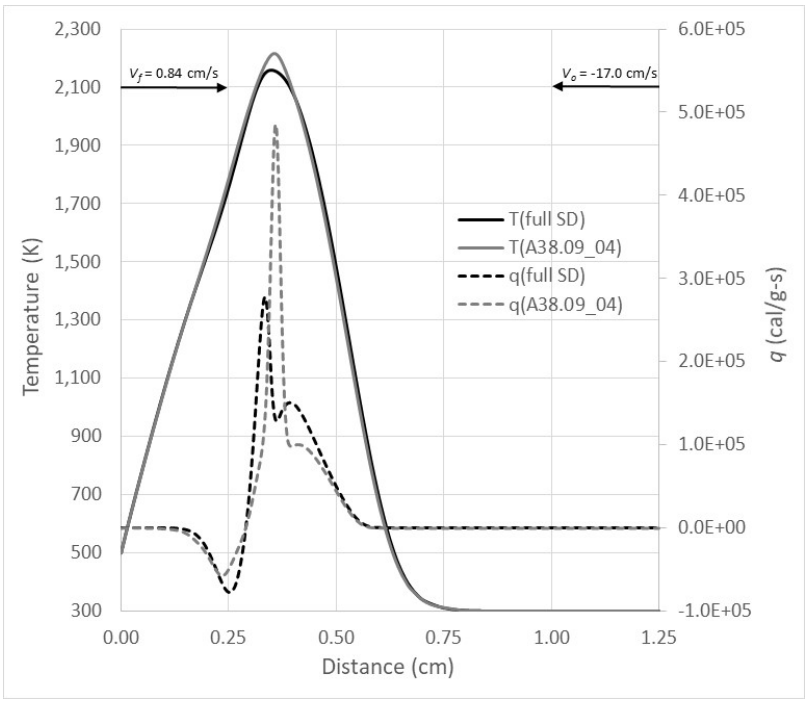

Fig. 5 Comparison of T and $\dot{q}_{mass}$ vs. distance plots obtained from SD- and A38.09_04-based OFDF solutions: P = 1.0 atm. O/F = 18.1, T_{fuel} = 500 K

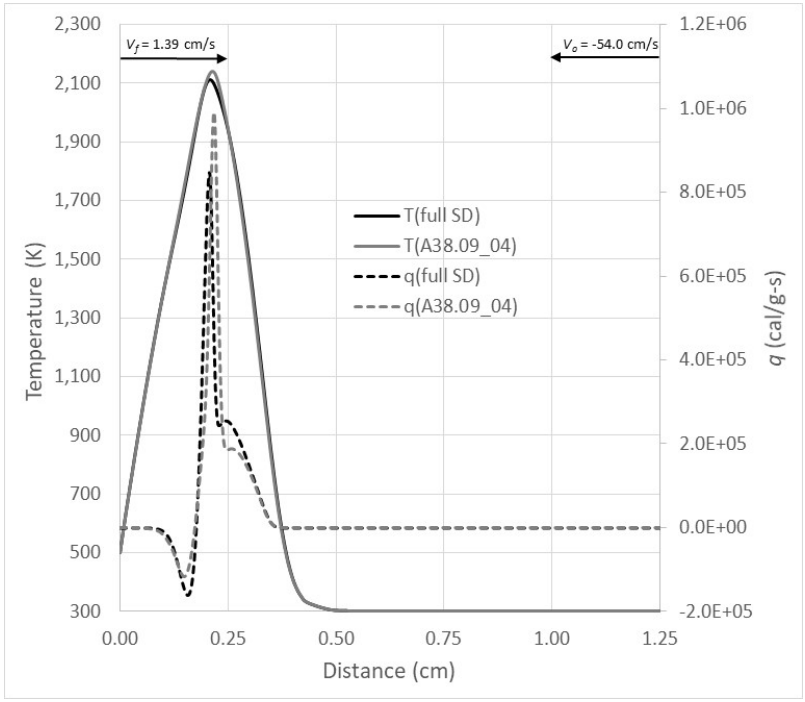

Fig. 6 Comparison of T and $\dot{q}_{mass}$ vs. distance plots obtained from SD- and A38.09_04-based OFDF solutions: P = 1.0 atm, O/F = 34.6, T_{fuel} = 500 K

As mentioned in the introduction, one of my concerns about using an HR-simulation-based TMM implementation to create a mechanism for an SFRJ combustor model was that I could not expect the evolution of a chemical composition in an HR simulation to mirror the evolution of the chemical composition found near the burning surface of a fuel grain. Nevertheless, given how sharp and featureless the (single) exothermic transient was in each of the three HR simulations that were the basis for the reduction protocol, the structure exhibited in the $\dot{q}_{mass}$ versus distance plots obtained from the OFDF simulations was surprising.

As for A38.09_04's ability to mimic the SD mechanism in these simulations, the A38.09_04-based $\dot{q}_{mass}$ versus distance plots qualitatively reproduced the SD-mechanism-based plots. However, the quantitative agreements between them were not as good as I had expected/hoped they would be. (My hope was that they would be within the MADs employed for the reduction process.) Nonetheless, from the standpoint of modeling SFRJ combustor dynamics, there was reason to be optimistic. The *T* versus distance plots produced with the two mechanisms did agree reasonably well, suggesting (based on the relationship between *r* and dT/dx at the fuel inlet expressed in Eq. 5) that models based on A38.09_04 would predict regression rates similar to those produced with the SD mechanism.

The OFDF simulation at 0.4 atm that did not yield a $\dot{q}_{mass}$ versus distance plot with the general features observed in Figs. 4–6 is shown in Fig. 7. It was produced for a system with an O/F at the low end of the range of interest. There was only one exothermic transient, and there was no endothermic transient. As found in Figs. 4–6, the agreement between the $\dot{q}_{mass}$ versus distance plots produced with the SD mechanism and with A38.09_04 was not as good as hoped. But the agreement between the *T* versus distance plots adjacent to the fuel inlet was (again) encouraging.

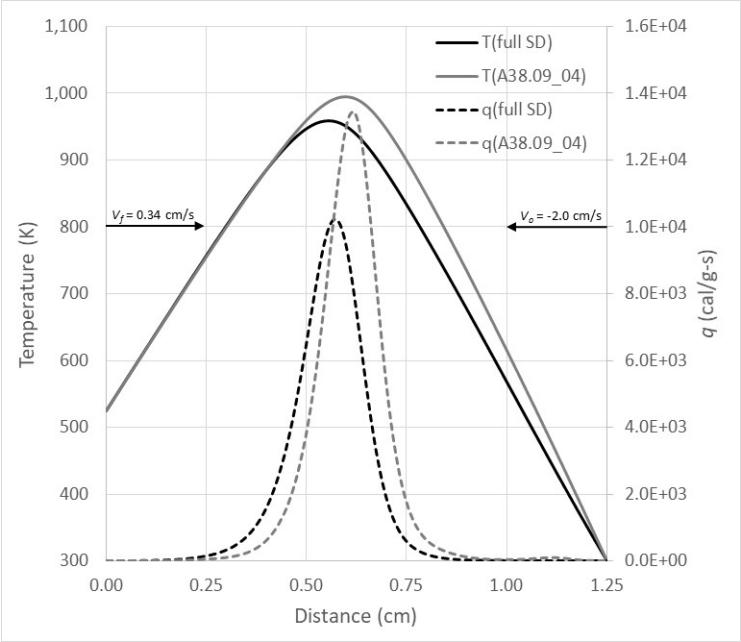

Fig. 7 Comparison of T and $\dot{q}_{mass}$ vs. distance plots obtained from SD- and A38.09_04-based OFDF solutions: P = 0.4 atm, O/F = 5.4, T_{fuel} = 525 K

It should also be noted that the maximum temperature (T_{max}) reached in this simulation was 960 K, and as such, was far lower than the 1800 K or more observed in all the other simulations. It suggests the system was near extinction conditions. It also suggests that the program may have been unable to find a nontrivial solution for the problem I posed in which the system's pressure was 0.3 atm because it was closer to (or at) extinction conditions.

Plots of T and $\dot{q}_{mass}$ versus distance obtained from a solution to a problem for a system at 6.2 atm is shown in Fig. 8. Unlike the $\dot{q}_{mass}$ versus distance plots obtained from solutions for systems at 1 atm, the analogous SD-mechanism-based plot in Fig. 8 exhibited two $\dot{q}_{mass}^{min}$ and only one $\dot{q}_{mass}^{max}$. (Plots obtained from simulations involving the other two 6.2 atm-V_{ox} combinations exhibited the same general features; see Appendix C.) The plot produced with A38.09_04 exhibited the two $\dot{q}_{mass}^{min}$ produced with the SD mechanism, but had two $\dot{q}_{mass}^{max}$. (Indeed, this plot evokes the plots shown in Figs. 4–6.) Nonetheless, the T versus distance plots produced with the two mechanisms were very similar, particularly on the fuel side, presaging that A38.09_04-based regression rate predictions would be similar to those produced with the SD mechanism.

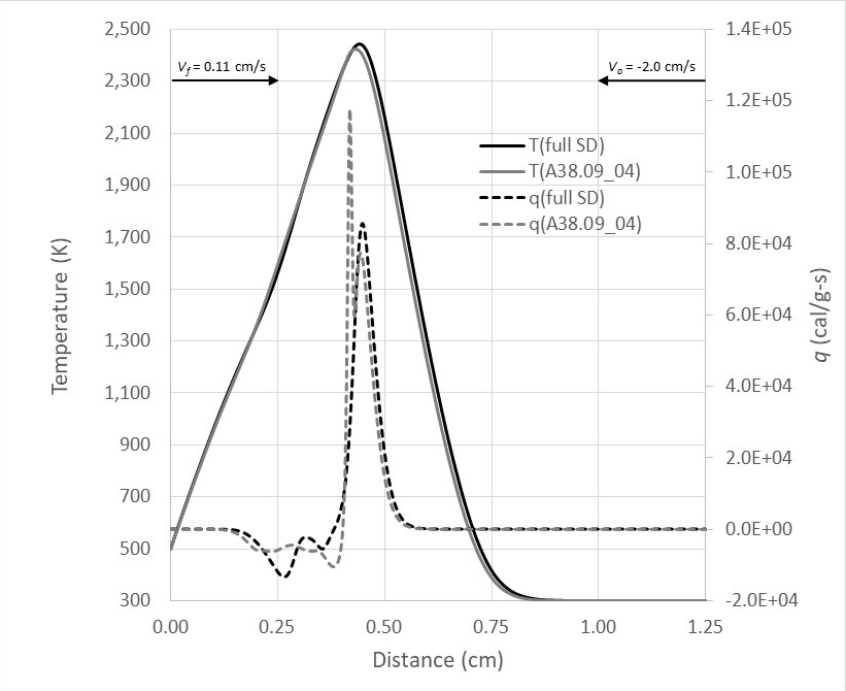

Fig. 8 Comparison of T and $\dot{q}_{mass}$ vs. distance plots obtained from SD- and A38.09_04-based OFDF solutions: P = 6.2 atm, O/F = 18.5, T_{fuel} = 500 K

With respect to A38.09_04's ability to mimic the SD mechanism within the prescribed parameter space, I was also interested in whether any species in the SD mechanism that was not in A38.09_04 would reach a significant concentration. Therefore, mole fraction versus distance data for all such species were plotted for all 18 P-V_{ox}-T_{fuel} cases. The only species that consistently reached a mole fraction that exceeded 1.0E-5 (or 0.001%) was "C3H3". (I assume it is the propargyl radical.) A representative plot, which was obtained from the solution for the P=6.2 atm, V_{ox} = 2 cm/s, T_{fuel} = 500 K problem (Fig. 8) is shown in Fig. 9. C3H3's mole fraction peaks at about the same location as the $\dot{q}_{mass}^{min}$ associated with the endothermic transient.

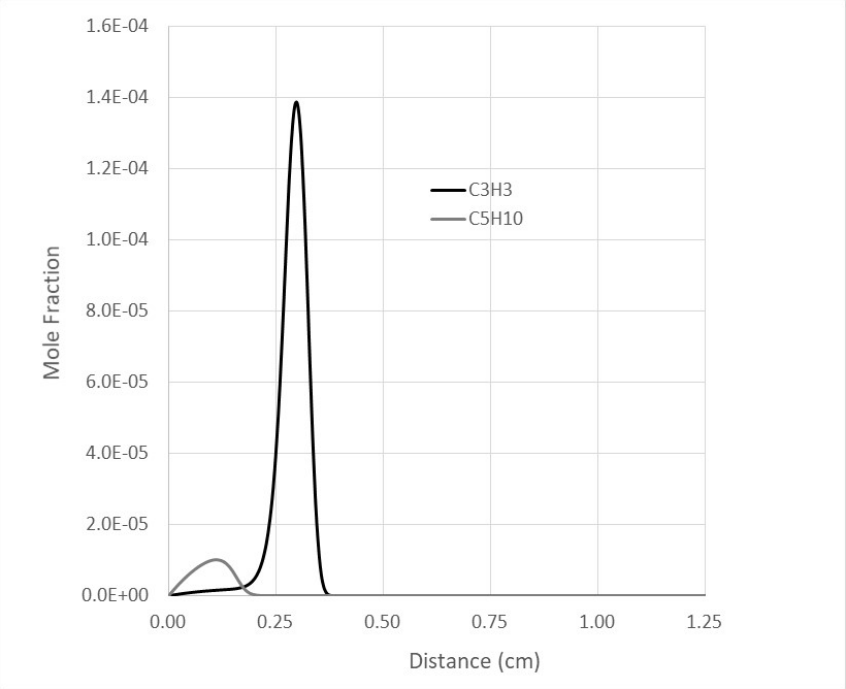

Fig. 9 Results from SD-mechanism-based solution for the OFDF problem with P = 6.2 atm, V_{ox} = 2 cm/s, and T_{fuel} = 500 K: mole fraction vs. distance plots for species that are not in A38.09_04 whose mole fraction at some point exceeded 1.0E-5. (Compare to Fig. 8.)

Additional analysis was not undertaken to determine whether the inclusion of C3H3 (and reactions that connected it to the network) would have led to better agreement between SD- and A38.09_04-based $\dot{q}_{mass}$ versus distance plots. (I assumed it would.) However, all other findings of this study suggested that, from the standpoint of modeling SFRJ combustor dynamics, obtaining better agreement between full- and skeletal-mechanism-based $\dot{q}_{mass}$ versus distance plots was not necessary.

The only SD-mechanism-based OFDF simulations in which the mole fraction of C3H3 did not at some point exceed 1.0E-5 were those in which P was 0.4 atm and V_{ox} was 2.0 cm/s. There were, however, five non-A38.09_04 species that had a mole fraction that at some point exceeded 1.0E-4, with CH3CHO (acetaldehyde) exceeding 3.5E-3 (Fig. 10). Again, I did not investigate whether the inclusion of these five species (and reactions that coupled them to the network) would have led to better agreements between the SD- and A38.09_04-based $\dot{q}_{mass}$ versus distance plots and T_{max}. If one wishes to predict extinction limits, an expansion of a reduced mechanism to include such species may be advisable/warranted.

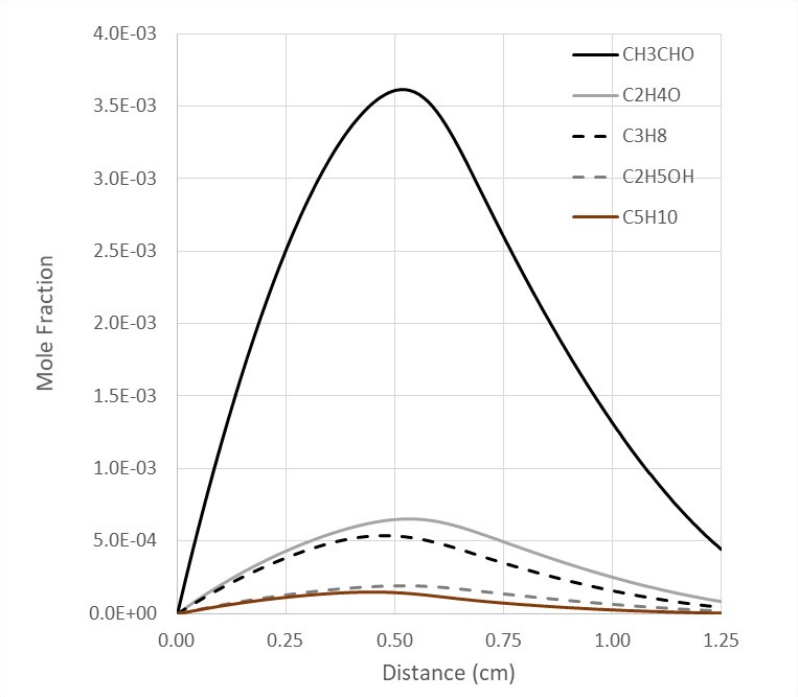

Fig. 10 Results from SD-mechanism-based solution for the OFDF problem with P = 0.4 atm, V_{ox} = 2 cm/s, and T_{fuel} = 525 K: mole fraction vs. distance plots for species that are not in A38.09_04 whose mole fraction at some point exceeded 1.0E-5. (Compare to Fig. 7.)

To corroborate the visual evidence that the temperature gradients produced with the SD mechanism and with A38.09_04 were similar near the fuel inlet, the temperature gradient at the second grid point $[(dT/dx)_{j=2}]$ was calculated via a central difference formula. The results are shown in Table 2. The largest difference was approximately 10%, and most were much smaller than that.

Table 2 Comparison of SD- and A38.09_04-based OFDF simulation results produced for various P-V_{ox}-T_{fuel} combinations: $(dT/dx)_{j=2}$, T_{max}, and r [a]

P—T_{fuel}	V_{ox} = 1 cm/s			V_{ox} = 2 cm/s			V_{ox} = 17 cm/s			V_{ox} = 54 cm/s		
Mechanism	$\left(\frac{dT}{dx}\right)_{j=2}$	T_{max}	r	$\left(\frac{dT}{dx}\right)_{j=2}$	T_{max}	r	$\left(\frac{dT}{dx}\right)_{j=2}$	T_{max}	r	$\left(\frac{dT}{dx}\right)_{j=2}$	T_{max}	r
	K/cm	**K**	**cm/s**	**K/cm**	**K**	**cm/s**	**K/cm**	**K**	**cm/s**	**K/cm**	**K**	**cm/s**
0.4 atm—500 K				O/F=5.4[b]			O/F=10.1			O/F=20.3		
SD				9.43E+02	959	1.9E-04	4.48E+03	2062	8.8E-04	7.09E+03	2004	1.4E-03
A38.09_04				9.41E+02	995	1.9E-04	4.44E+03	2082	8.6E-04	7.02E+03	2015	1.4E-03
0.4 atm—650 K				O/F=6.5			O/F=12.0			O/F=24.0		
SD				6.54E+02	1037	1.6E-04	3.09E+03	2078	7.4E-04	4.92E+03	2022	1.2E-03
A38.09_04				6.36E+02	1043	1.5E-04	3.04E+03	2103	7.3E-04	4.86E+03	2033	1.2E-03
1.0 atm—500 K				O/F=6.6			O/F=18.1			O/F=34.6		
SD				2.00E+03	1820	3.9E-04	6.26E+03	2158	1.2E-03	1.04E+04	2112	2.0E-03
A38.09_04				1.96E+03	1841	3.9E-04	6.24E+03	2216	1.2E-03	1.04E+04	2142	2.0E-03
1.0 atm—650 K				O/F = 8.3			O/F=21.7			O/F=40.5		
SD				1.30E+03	1804	3.1E-04	4.28E+03	2175	1.0E-03	7.20E+03	2131	1.7E-03
A38.09_04				1.25E+03	1821	3.0E-04	4.22E+03	2237	1.0E-03	7.13E+03	2164	1.7E-03
6.2 atm—500 K	O/F=10.6			O/F=18.5			O/F=52.5					
SD	3.90E+03	2457	7.7E-04	5.10E+03	2445	1.0E-03	1.32E+04	2382	2.6E-03			
A38.09_04	3.77E+03	2435	7.4E-04	4.94E+03	2465	9.6E-04	1.30E+04	2386	2.6E-03			
6.2 atm—650 K	O/F=13.0			O/F=19.9			O/F=63.3					
SD	2.77E+03	2472	6.5E-04	3.41E+03	2461	8.1E-04	9.08E+03	2401	2.2E-03			
A38.09_04	2.49E+03	2450	6.0E-04	3.28E+03	2441	7.8E-04	8.91E+03	2404	2.1E-03			

[a] The O/Fs shown are based on the solutions produced with the SD mechanism.
[b] T_{fuel} = 525 K.

4.2.3 Regression Rate Predictions

Table 2 also presents the regression rates predicted for each of the P-V_{ox}-T_{fuel} cases discussed in the previous section. The predictions are compared graphically in Fig. 11. Considering first the SD-mechanism-based predictions, I was struck by two outcomes. One was that for a given P-V_{ox} (pair), the difference between the rates produced when T_{fuel} was 500 K and when it was 650 K was not particularly significant. Generally, the rate predicted when T_{fuel} was 500 K was about 20% higher than when it was 650 K. This suggested that (depending on the application and objective) one might not need to be overly careful in formulating a representation (e.g., a pyrolysis law) to calculate the rate of the condensed-phase-to-gas-phase conversion process. (A similar insensitivity of CYCLOPS-based burning rate predictions to the parameterization of the model's pyrolysis law was previously observed for ammonium perchlorate [McQuaid and Chen 2014].) Because the burning rate predictions were relatively insensitive to T_{fuel}'s value, only results produced for problems in which T_{fuel} was 500 K are discussed in the remainder of this section.

I was also initially surprised by how low the predictions were. The largest was 2.6E-03 cm/s (0.026 mm/s = 1.6 mm/min). Based on measured regression rates in figures published by Shark et al. (2014) and Hedman (2016), I was expecting the predictions to be an order of magnitude higher. However, further consideration of the conditions under which the measured rates were produced assuaged my concern. In Shark et al.'s experiments, the oxidizer was pure O_2 (not air), and V_{ox} (calculated based on the flow rate [7 to 50 standard liters per minute] and the nozzle diameter [0.75 mm] reported) was from 260 to 1900 cm/s. Once that was appreciated, the difference between the regression rates observed in those experiments and the rates predicted in this investigation could be rationalized.

As for Hedman's data, further consideration of them was actually encouraging. In his experiments, the energy source for HTPB's pyrolysis was radiation from a CO_2 laser, and he measured regression rates for fluences from 50 to 200 W/cm^2. At the highest regression rate predicted in the current study (again 0.026 mm/s), the (thermal) fluence was only 6 W/cm^2. Extrapolating Hedman's data back to 6 W/cm^2, I found that the predicted rate could well be reasonable.

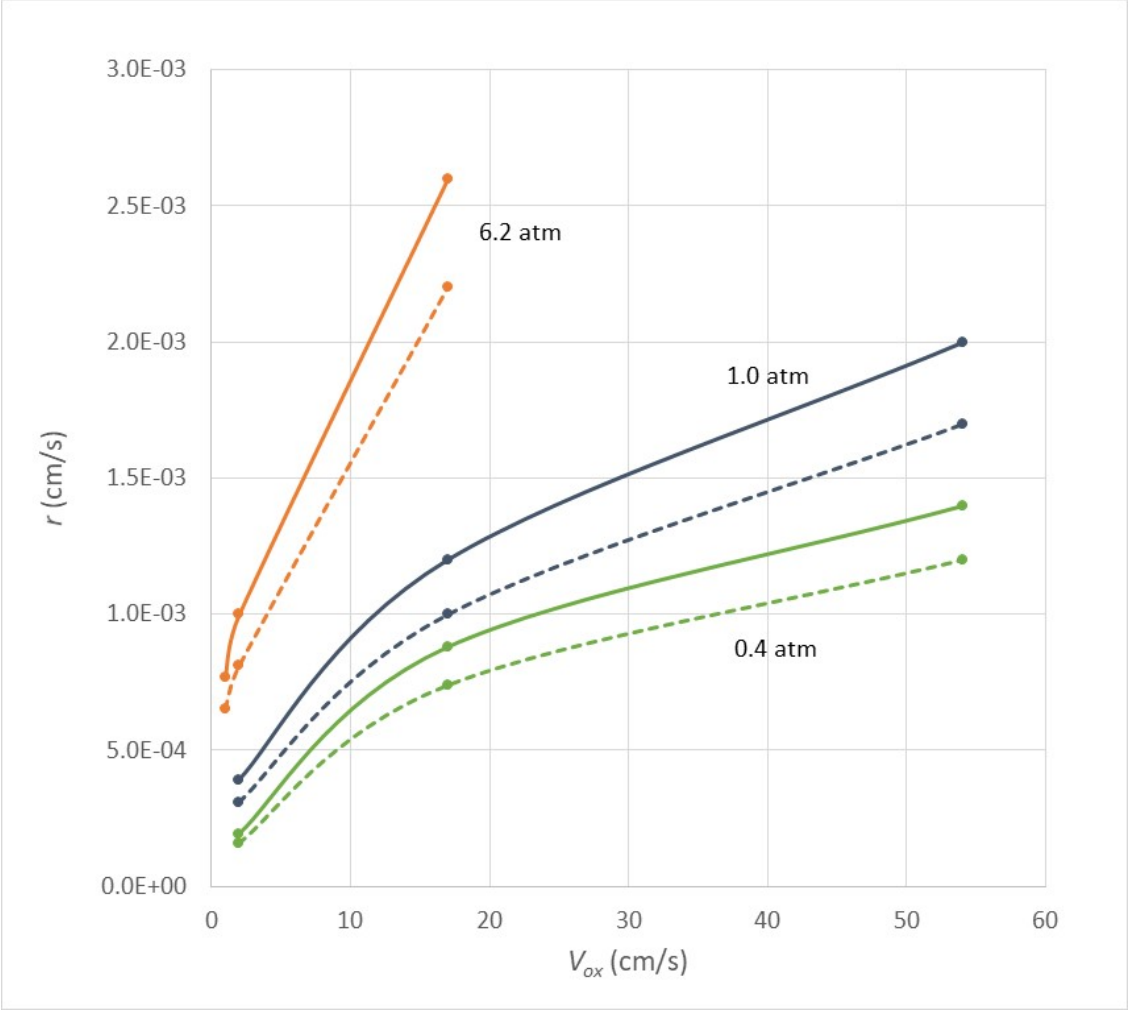

Fig. 11 SD-mechanism-based regression rate predictions as a function of P and V_{ox}. Solid lines correspond to T_{fuel} = 500 K; dashed lines correspond to T_{fuel} = 650 K

Finally, I imagined the simulation at 1 atm with an opposed flow of air having a velocity of 2 cm/s was similar to a (wax) candle burning in a quiescent room. The prediction for that simulation (0.23 mm/min) would thus predict that a candle burning for 1 h would regress about 0.55 inches. As such, it conformed to my expectation for that scenario. To corroborate that expectation, I performed a crude experiment, burning for 1 h a 0.75-inch-diameter LUMINESSENCE 5-h emergency candle that I bought at a dollar store. (The candle had a waxy feel, but otherwise its chemical composition was unknown.) The candle was approximately 16 cm (0.6 inch) shorter at the end of the hour. Although I cannot dismiss the possibility that the reasonable agreement between the measured and predicted rates was coincidental, it was nonetheless encouraging, suggesting that the predicted rates may prove to be within a factor of 2 of those that will be measured.

As for the differences in the SD- and A38.09_04-based regression rate predictions, they (not surprisingly) mirrored the differences in $(dT/dx)_{j=2}$. The largest difference was 10%, and most were far smaller than that. Therefore, even if the SD mechanism proves to have shortcomings as a thermochemical kinetics basis for modeling either the proposed experiments or SFRJ combustor dynamics, the comparisons indicated that a HR-simulation-based TMM implementation has the potential to create from a valid representation a skeletal mechanism that is similarly valid.

5. Alternate TMM Implementation

Long cognizant that an HR-simulation-based TMM implementation might be a less than optimal approach for reducing a mechanism to model dynamics such as those in an SFRJ combustor, I developed and beta-tested an OFDF-simulation-based TMM implementation, but have yet to apply it to a "real" problem. (The beta test involved reducing a mechanism for modeling H_2–O_2 combustion based on trial-mechanism-based solutions for several variations of the OFDF problem provided as an example in the OPPDIF manual [Lutz et al. 1997].) Similar to the HR-simulation-based TMM implementation employed for this study, its screening algorithm compared $\dot{q}_{mass}^{max}$ and $\dot{q}_{vol}^{max}$, the locations at which those maxima occurred (d_{mass}^{max} and d_{vol}^{max}, respectively), and T_{max}. However, as shown in this study and a prior one (McQuaid et al. 2019), it is possible for a reduced-mechanism-based OFDF simulation to reasonably reproduce key features of one produced with a full mechanism, including $(dT/dx)_{j=2}$, T_{max}, and T_{max}'s location (d_T^{max}), without there being good agreement between their respective $\dot{q}_{mass}^{max}$, $\dot{q}_{vol}^{max}$, d_{mass}^{max}, and d_{vol}^{max} values. Thus, the standard MADs that have been specified (to date) for the values of analogous parameters in HR-simulation-based TMM implementations appear to be significantly more restrictive than necessary for an OFDF-simulation-based implementation. If so, they would result in reduced mechanisms being larger than necessary. Therefore, I plan to reprogram the screening algorithm so that it only compares $(dT/dx)_{j=2}$, T_{max}, and d_T^{max} values. Covering the parameter space expected in the proposed experiments, the 18 OFDF simulations whose results are summarized in Table 2 will be the basis for that reduction effort.

6. Summary and Conclusions

To evaluate the potential of an HR-simulation-based implementation of the TMM to produce skeletal/reduced finite-rate chemical kinetics mechanisms that are valid for use in physics-based models of SFRJ combustor dynamics, one was formulated and employed to reduce the SD mechanism to skeletal versions that will be applicable to simulating proposed opposed-flow burner experiments involving HTPB and N_2–O_2 mixtures. Numerous candidates were generated via a relatively rudimentary protocol, and the smallest one was vetted for the application. Named A38.09_04, it comprised 63 reactions and 33 species; the SD mechanism comprised 323 reactions and 67 species. It was confirmed that when A38.09_04 was substituted for the SD mechanism in HR simulations with initial conditions similar to those expected to be realized in the gas near HTPB's pyrolyzing surface, the T and $\dot{q}_{mass}$ versus t histories derived from the solutions were in reasonable agreement with those from derived from the corresponding SD-mechanism-based solution.

In addition, the SD mechanism and A38.09_04 were employed as bases for OFDF simulations with characteristics similar to those expected to be realized in the proposed experiments. Key features of SD-mechanism-based simulations, including the temperature gradient adjacent to the fuel inlet, T_{max}, and T_{max}'s location, were found to be reasonably reproduced when A38.09_04 was employed as the basis. An ability to predict HTPB's regression rate as a function of P, V_{ox}, and T_{fuel} on the basis of the solutions to such problems was also demonstrated, and A38.09_04-based predictions were in reasonable agreement with those produced with the SD mechanism. The evaluation thus indicated that an HR-simulation-based TMM implementation can produce skeletal mechanisms that are valid for use in physics-based SFRJ combustor models.

7. References

Beckstead MW, Puduppakkam K, Thakre P, Yang V. Modeling of combustion and ignition of solid propellants ingredients. Progress in Energy and Combustion Science. 2007;33:497–551.

Bojko B. Naval Air Warfare Center, China Lake, CA. Email communication, 2019 July 24.

Chen CC, McQuaid MJ. Thermochemical and kinetic studies of the pyrolysis of hydroxyl-terminated polybutadiene (HTPB). Presented at the 43rd JANNAF Combustion Subcommittee Meeting; 2009 Dec 7–11; La Jolla, CA.

Chen CC, McQuaid MJ. Thermochemistry and kinetics modeling of hydroxyl-terminated polybutadiene-red fuming nitric acid (HTPB-RFNA) systems. Presented at the 5th JANNAF Liquid Propulsion Subcommittee Meeting; 2010 May 3–7; Colorado Springs, CO.

Chen CC, McQuaid MJ. Thermochemistry and kinetics modeling of the oxidation of hydroxyl-terminated polybutadiene in air. Presented at the 44th JANNAF Combustion Subcommittee Meeting; 2011 Apr 18–22; Arlington, VA.

Chen CC, McQuaid MJ. Thermochemical and kinetics modeling pertaining to AP-HTPB composite propellant combustion. Presented at the 39th JANNAF Propellant and Explosives Development and Characterization Meeting; 2015 Dec 7–10, Salt Lake City, UT.

Chen CC, McQuaid MJ. A skeletal, gas-phase, finite-rate, chemical kinetics mechanism for modeling the deflagration of ammonium perchlorate-hydroxyl-terminated polybutadiene composite propellants. Aberdeen Proving Ground (MD): Army Research Laboratory (US); 2016 Apr. Report No.: ARL-TR-7655.

Chen CC, McQuaid MJ. A skeletal finite-rate chemical kinetics mechanism for modeling HTPB-air combustion in a gun-launched solid-fuel ramjet combustor. Aberdeen Proving Ground (MD): CCDC Army Research Laboratory (US); 2020 Jan. Report No.: ARL-TR-8891.

Chen CC, Anderson WR, McQuaid MJ. Computationally based predictions for the burning rates and flame structures of nitroglycerin doped with various small molecules. Aberdeen Proving Ground (MD): CCDC Army Research Laboratory (US); 2019 June. Report No.: ARL-TR-8721.

Gariani G, Maggi F, Galfetti L. Numerical simulation of HTPB combustion in a 2D hybrid slab combustor. Acta Astronautica. 2011;69:289–296.

Hedman TD. Radiation-induced pyrolysis of solid fuels for ramjet application. Propulsion and Power Research. 2016;5:87-96.

Kee RJ, Rupley FM, Miller JA, Coltrin ME, Grcar JF, Meeks E, Moffat HK, Lutz AE, Dixon-Lewis G, Smooke MD, et al. CHEMKIN Collection, release 3.7. San Diego (CA): Reaction Design, Inc.; 2002.

Kotlar AJ. A general approach for the reduction of chemical reaction mechanisms. I: methodology and application to MMH-RFNA. Presented at the 5th JANNAF Liquid Propulsion Subcommittee Meeting; 2010 May 3–7; Colorado Springs, CO.

Krishnan S, George P. Solid fuel ramjet combustor design. Progress in Aerospace Sciences. 1998;34:219–256.

Kumar CP, Kumar A. Effect of swirl on the regression rate of hybrid rocket motors. Aerospace Science and Technology. 2013;29:92–99.

Li S, Petzold LR. Design of new DASPK for sensitivity analysis. Santa Barbara (CA): Department of Computer Science, University of California; 1999. Report No.: TRC99-28.

Lutz, AE, Kee RJ, Grcar JF, Rupley FM. OPPDIF: A Fortran program for computing opposed-flow diffusion flames. Albuquerque (NM): Sandia National Laboratories; 1997. Report No.: SAND96-8243.

McDonald B, Rice J, Stewart J. Mechanical and thermodynamic characterization of a copolymer of LP-33 polysulfide and hydroxyl terminated polybutadiene for solid fuel ramjet applications. Combustion and Flame. 2017;184:11–19.

McQuaid MJ. The trial mechanism method for chemical kinetics mechanism reduction: an approach to developing mechanisms with wider ranges of applicability. Presented at the 7th JANNAF Liquid Propulsion Subcommittee Meeting; 2013a Apr 29–May 2; Colorado Springs, CO.

McQuaid MJ. Chemical kinetics mechanism reduction based on principal component analysis: development and testing of some new implementations. Aberdeen Proving Ground (MD): Army Research Laboratory (US); 2013b May. Report No.: ARL-TR-6449.

McQuaid MJ, Chen CC. Modeling the deflagration of ammonium perchlorate at pressures from 300 to 30000 psia. Part II: considerations besides the gas-phase, finite rate chemical kinetics mechanism. Presented at the 46th JANNAF Combustion Subcommittee Meeting; 2014 Dec 8–11; Albuquerque, NM.

McQuaid MJ, Chen CC, Veals JD. Modeling ammonia borane-red fuming nitric acid combustion. Part 2: detailed finite-rate chemical kinetics mechanism reduction and validation. Presented at the 49th JANNAF Combustion Subcommittee Meeting; 2019 June 3–7; Dayton, OH.

Miller MS, Anderson WR. Energetic-material combustion modeling with elementary gas-phase reactions: a practical approach. In: Yang V, Brill TB, Ren WZ, editors. Solid propellant combustion chemistry, combustion, and motor interior ballistics, progress in astronautics and aeronautics. Reston (VA): AIAA; 2000;185:501–531.

Miller MS, Anderson WR. Burning-rate predictor for multi-ingredient propellants: nitrate-ester propellants. J Propul Power. 2004;20(3):440–454.

Morinigo JA, Hermida-Quesada J. Evaluation of reduced-order kinetics models for HTPB-oxygen combustion using LES. Aerospace Science and Technology. 2016;58:358–368.

Moshammer K, Seidel L, Wang Y, Selim H, Sarthy SM, Mauss F, Hansen N. Aromatic ring formation in opposed diffusive 1,3-butadiene flames. Proceedings of the Combustion Institute. 2017;6:947–955.

Nusca MJ, Minnicino M, Chen CC, Isert S, McBain A. Multidisciplinary gun-launched solid fuel ramjet (SFRJ) projectile study – initial CFD modeling results. Presented at the 49th JANNAF Combustion Subcommittee Meeting; 2019 3–7 June; Dayton, OH.

Reynolds WC. The element potential method of chemical equilibrium analysis: implementation in the interactive program STANJAN, version 3.0. Stanford (CA): Dept. of Mechanical Engineering, Stanford University; 1986.

Stone C. Summary of user productivity enhancement, technology transfer, and training (PETTT) refactoring assistance for chemical kinetics analysis tools at CCDC Army Research Laboratory. Aberdeen Proving Ground (MD): CCDC Army Research Laboratory (US); 2020 Jan. Report No.: ARL-CR-0843.

Sun X, Tian H, Yu N, Cai G. Regression rate and combustion performance investigation of aluminum metallized HTPB/98HP hybrid rocket motor with numerical simulation. Aerospace Science and Technology. 2015;42:287–296.

Appendix A. Representative Input Deck for Opposed-Flow Diffusion Flame Simulations

The program employed to set up and solve the opposed-flow diffusion flame problems discussed in this report was a slight variation of the CHEMKIN program OPPDIF.[1] Problems were formulated via an input "deck". Table A-1 is representative of all that were submitted. Each line began with a keyword that prompted the program to set the value of some parameter (or parameters). For their definitions, see the OPPDIF manual.[1] Only the values of the parameters set via PRES-, VFUE-, VOXI-, and TFUE-led lines were varied. For any parameter value not set via the input deck, the default prescribed by the foundational program was used.[1] Searches for solutions to new problems were facilitated by providing initial estimates for state variables based on values for them in a restart file corresponding to a simulation defined with different PRES-, VFUE-, VOXI-, and/or TFUE-led lines. It was observed that as long as the differences between the values of the parameters specified via these lines and those that produced the restart file were not greater than about 20%, the program would solve the new problem fairly readily.

Table A-1 Representative input deck for opposed-flow diffusion flame simulations

```
RSTR
MIX
ENRG
PRES 0.4
VFUE 0.3450E+00
VOXI 2.0000E+00
TFUE 525.
TOXI 300.
XEND 1.250
IRET 20
UFAC 2.
SFLR -1.E-4
TIME 200 1.E-6
TIM2 200 1.E-6
GRAD 0.1
CURV 0.5
FUEL C4H6 1.00
OXID N2   0.78
OXID O2   0.21
OXID AR   0.01
KOUT C4H6 N2 O2 H2O CO CO2
RTOL 1.E-3
ATOL 1.E-6
ATIM 1.E-6
RTIM 1.E-3
END
```

[1] Lutz, AE, Kee RJ, Grcar JF, Rupley FM. OPPDIF: A Fortran program for computing opposed-flow diffusion flames. Albuquerque (NM): Sandia National Laboratories; 1997. Report No.: SAND96-8243.

Appendix B. A38.09_04's Species, Reactions, and Reaction Rate-Coefficient Parameterizations

Table B-1 lists the species, elementary reactions and reaction rate-coefficient parameterizations that composed A38.09_04. The table was produced by a pre-commercial CHEMKIN III "preprocessor"/mechanism interpreter. All the data in the input files originated in the San Diego mechanism. They were downloaded from https://web.eng.ucsd.edu/mae/groups/combustion/mechanism.html.

Table B-1 Species, elementary reactions and reaction rate-coefficient parameters that composed A38.09_04

```
CHEMKIN-III GAS-PHASE MECHANISM INTERPRETER:
DOUBLE PRECISION Vers. 6.3 97/01/25
Copyright 1995, Sandia Corporation.
The U.S. Government retains a limited license in this software.
                         --------------------
                         ELEMENTS     ATOMIC
                         CONSIDERED   WEIGHT
                         --------------------
                          1. N       14.0067
                          2. AR      39.9480
                          3. HE      4.00260
                          4. H       1.00797
                          5. O       15.9994
                          6. C       12.0112
                         --------------------
--------------------------------------------------------------------------------
                         C
                       P H
                       H A
                       A R
SPECIES                S G  MOLECULAR  TEMPERATURE  ELEMENT COUNT
CONSIDERED             E E  WEIGHT     LOW    HIGH  N  AR HE H  O  C
--------------------------------------------------------------------------------
  1. N2                G  0   28.01340   300   5000   2  0  0  0  0  0
  2. AR                G  0   39.94800   300   5000   0  1  0  0  0  0
  3. HE                G  0    4.00260   300   5000   0  0  1  0  0  0
  4. H                 G  0    1.00797   300   5000   0  0  0  1  0  0
  5. O2                G  0   31.99880   300   5000   0  0  0  0  2  0
  6. OH                G  0   17.00737   300   5000   0  0  0  1  1  0
  7. O                 G  0   15.99940   300   5000   0  0  0  0  1  0
  8. H2                G  0    2.01594   300   5000   0  0  0  2  0  0
  9. H2O               G  0   18.01534   300   5000   0  0  0  2  1  0
 10. HO2               G  0   33.00677   300   5000   0  0  0  1  2  0
 11. H2O2              G  0   34.01474   300   5000   0  0  0  2  2  0
 12. CO                G  0   28.01055   300   5000   0  0  0  0  1  1
 13. CO2               G  0   44.00995   300   5000   0  0  0  0  2  1
 14. HCO               G  0   29.01852   300   5000   0  0  0  1  1  1
 15. CH3               G  0   15.03506   300   5000   0  0  0  3  0  1
 16. CH4               G  0   16.04303   300   5000   0  0  0  4  0  1
 17. CH2O              G  0   30.02649   300   5000   0  0  0  2  1  1
 18. T-CH2             G  0   14.02709   300   5000   0  0  0  2  0  1
 19. C2H4              G  0   28.05418   300   5000   0  0  0  4  0  2
 20. CH3O              G  0   31.03446   300   5000   0  0  0  3  1  1
 21. C2H5              G  0   29.06215   300   5000   0  0  0  5  0  2
 22. C2H6              G  0   30.07012   300   5000   0  0  0  6  0  2
 23. C2H2              G  0   26.03824   300   5000   0  0  0  2  0  2
 24. C2H3              G  0   27.04621   300   5000   0  0  0  3  0  2
 25. CH2CHO            G  0   43.04561   300   5000   0  0  0  3  1  2
 26. HCCO              G  0   41.02967   300   5000   0  0  0  1  1  2
 27. CH2CO             G  0   42.03764   300   5000   0  0  0  2  1  2
 28. CH2OH             G  0   31.03446   300   5000   0  0  0  3  1  1
 29. C3H4              G  0   40.06533   300   5000   0  0  0  4  0  3
 30. C3H5              G  0   41.07330   300   5000   0  0  0  5  0  3
 31. C3H6              G  0   42.08127   300   5000   0  0  0  6  0  3
 32. C4H8              G  0   56.10836   300   5000   0  0  0  8  0  4
 33. C4H6              G  0   54.09242   300   3000   0  0  0  6  0  4
--------------------------------------------------------------------------------
```

	REACTIONS CONSIDERED			(k = A T**b exp(-E/RT)) A	b	E
1.	H+O2<=>OH+O			3.52E+16	-0.7	17069.8
2.	H2+O<=>OH+H			5.06E+04	2.7	6290.6
3.	H2+OH<=>H2O+H			1.17E+09	1.3	3635.3
4.	H2O+O<=>2OH			7.00E+05	2.3	14548.3
5.	H+OH+M<=>H2O+M			4.00E+22	-2.0	0.0
	AR	Enhanced by	3.800E-01			
	HE	Enhanced by	3.800E-01			
	H2	Enhanced by	2.500E+00			
	H2O	Enhanced by	1.200E+01			
	CO	Enhanced by	1.900E+00			
	CO2	Enhanced by	3.800E+00			
6.	H+O2(+M)<=>HO2(+M)			4.65E+12	0.4	0.0
	AR	Enhanced by	7.000E-01			
	HE	Enhanced by	7.000E-01			
	H2	Enhanced by	2.500E+00			
	H2O	Enhanced by	1.600E+01			
	CO	Enhanced by	1.200E+00			
	CO2	Enhanced by	2.400E+00			
	C2H6	Enhanced by	1.500E+00			
	Low pressure limit:	0.57500E+20	-0.14000E+01	0.00000E+00		
	TROE centering:	0.50000E+00	0.10000E-29	0.10000E+31		
7.	HO2+H<=>2OH			7.08E+13	0.0	294.9
8.	HO2+H<=>H2+O2			1.66E+13	0.0	822.9
9.	HO2+O<=>OH+O2			2.00E+13	0.0	0.0
10.	HO2+OH<=>H2O+O2			7.00E+12	0.0	-1094.7
	Declared duplicate reaction...					
11.	HO2+OH<=>H2O+O2			4.50E+14	0.0	10929.7
	Declared duplicate reaction...					
12.	2OH(+M)<=>H2O2(+M)			9.55E+13	-0.3	0.0
	AR	Enhanced by	7.000E-01			
	HE	Enhanced by	4.000E-01			
	H2	Enhanced by	2.500E+00			
	H2O	Enhanced by	6.000E+00			
	H2O2	Enhanced by	6.000E+00			
	CO	Enhanced by	1.500E+00			
	CO2	Enhanced by	2.000E+00			
	Low pressure limit:	0.27600E+26	-0.32000E+01	0.00000E+00		
	TROE centering:	0.57000E+00	0.10000E+31	0.10000E-29		
13.	2HO2<=>H2O2+O2			1.03E+14	0.0	11042.1
	Declared duplicate reaction...					
14.	2HO2<=>H2O2+O2			1.94E+11	0.0	-1408.9
	Declared duplicate reaction...					
15.	H2O2+H<=>H2O+OH			1.00E+13	0.0	3585.1
16.	H2O2+OH<=>H2O+HO2			7.59E+13	0.0	7272.9
17.	CO+OH<=>CO2+H			4.40E+06	1.5	-740.9
18.	HCO+M<=>CO+H+M			1.86E+17	-1.0	17000.5
	H2	Enhanced by	1.900E+00			
	H2O	Enhanced by	1.200E+01			
	CO	Enhanced by	2.500E+00			
	CO2	Enhanced by	2.500E+00			
19.	HCO+O2<=>CO+HO2			7.58E+12	0.0	409.9
20.	HCO+CH3<=>CO+CH4			5.00E+13	0.0	0.0
21.	CH2O+H<=>HCO+H2			5.74E+07	1.9	2748.6
22.	CH2O+O<=>HCO+OH			3.50E+13	0.0	3513.4
23.	CH2O+OH<=>HCO+H2O			3.90E+10	0.9	406.3
24.	CH4+H<=>H2+CH3			1.30E+04	3.0	8037.8
25.	CH3+O<=>CH2O+H			8.43E+13	0.0	0.0
26.	CH3+HO2<=>CH3O+OH			5.00E+12	0.0	0.0
27.	2CH3<=>C2H5+H			3.16E+13	0.0	14698.9
28.	H+CH3(+M)<=>CH4(+M)			1.35E+14	0.1	87.7
	AR	Enhanced by	7.000E-01			
	H2	Enhanced by	2.000E+00			
	H2O	Enhanced by	1.600E+01			
	CO	Enhanced by	1.500E+00			
	CO2	Enhanced by	2.000E+00			
	CH4	Enhanced by	4.000E+00			
	Low pressure limit:	0.15900E+34	-0.47610E+01	0.24323E+04		
	TROE centering:	0.83400E+00	0.36800E+02	0.77800E+03	0.24643E+04	

```
29. T-CH2+O2<=>CO+OH+H                                6.58E+12    0.0     1491.4
30. CH3O+M<=>CH2O+H+M                                 7.78E+13    0.0    13513.4
    AR              Enhanced by    7.000E-01
    H2              Enhanced by    2.000E+00
    H2O             Enhanced by    6.000E+00
    CO              Enhanced by    1.500E+00
    CO2             Enhanced by    2.000E+00
    CH4             Enhanced by    2.000E+00
31. C2H5(+M)<=>C2H4+H(+M)                             1.11E+10    1.0    36768.6
    AR              Enhanced by    7.000E-01
    H2              Enhanced by    2.000E+00
    H2O             Enhanced by    6.000E+00
    CO              Enhanced by    1.500E+00
    CO2             Enhanced by    2.000E+00
    CH4             Enhanced by    2.000E+00
    Low pressure limit:  0.39900E+34 -0.49900E+01  0.40000E+05
    TROE centering:      0.16800E+00  0.12000E+04  0.10000E-29
32. C2H4+OH<=>C2H3+H2O                                5.53E+05    2.3     2963.7
33. C2H4+O<=>CH3+HCO                                  2.25E+06    2.1        0.0
34. C2H3+H<=>C2H2+H2                                  4.00E+13    0.0        0.0
35. C2H3+O2<=>CH2O+HCO                                1.70E+29   -5.3     6503.1
36. C2H3+O2<=>CH2CHO+O                                7.00E+14   -0.6     5262.4
37. C2H2+O<=>HCCO+H                                   4.00E+14    0.0    10659.7
38. CH2CO+H<=>CH3+CO                                  1.50E+09    1.4     2688.8
39. CH2CO+O<=>T-CH2+CO2                               2.00E+13    0.0     2294.5
40. HCCO+O2<=>CO2+CO+H                                1.40E+07    1.7     1001.4
41. CH2OH+O2<=>CH2O+HO2                               5.00E+12    0.0        0.0
42. CH2CO+OH<=>CH2OH+CO                               1.02E+13    0.0        0.0
43. CH2CHO<=>CH2CO+H                                  1.05E+37   -7.2    44340.3
44. CH2CHO+O2<=>CH2O+CO+OH                            3.00E+10    0.0        0.0
45. CH3+C2H2<=>C3H4+H                                 2.56E+09    1.1    13643.9
46. C3H4+H(+M)<=>C3H5(+M)                             4.00E+13    0.0        0.0
    Low pressure limit:  0.30000E+25 -0.20000E+01  0.00000E+00
    TROE centering:      0.80000E+00  0.10000E+31  0.10000E-29
47. C3H6+O<=>C2H5+HCO                                 3.50E+07    1.6     -972.8
48. C3H6+OH<=>C3H5+H2O                                3.10E+06    2.0     -298.3
49. C3H6+O<=>CH2CO+CH3+H                              1.20E+08    1.6      327.4
50. C3H6+H<=>C3H5+H2                                  1.70E+05    2.5     2492.8
51. C3H5+H(+M)<=>C3H6(+M)                             2.00E+14    0.0        0.0
    AR              Enhanced by    7.000E-01
    H2              Enhanced by    2.000E+00
    H2O             Enhanced by    6.000E+00
    CO              Enhanced by    1.500E+00
    CO2             Enhanced by    2.000E+00
    CH4             Enhanced by    2.000E+00
    C2H6            Enhanced by    3.000E+00
    Low pressure limit:  0.13300E+61 -0.12000E+02  0.59680E+04
    TROE centering:      0.20000E-01  0.10970E+04  0.10970E+04  0.68600E+04
52. C3H5+HO2<=>C3H6+O2                                2.66E+12    0.0        0.0
53. C3H5+HO2<=>OH+C2H3+CH2O                           3.00E+12    0.0        0.0
54. C2H3+CH3(+M)<=>C3H6(+M)                           2.50E+13    0.0        0.0
    AR              Enhanced by    7.000E-01
    H2              Enhanced by    2.000E+00
    H2O             Enhanced by    6.000E+00
    CO              Enhanced by    1.500E+00
    CO2             Enhanced by    2.000E+00
    CH4             Enhanced by    2.000E+00
    C2H6            Enhanced by    3.000E+00
    Low pressure limit:  0.42700E+59 -0.11940E+02  0.97705E+04
    TROE centering:      0.17500E+00  0.13410E+04  0.60000E+05  0.10140E+05
55. C3H6+H<=>C2H4+CH3                                 1.60E+22   -2.4    11185.5
56. C4H8<=>C3H5+CH3                                   1.00E+16    0.0    72896.8
57. C4H8+H<=>H2+C2H3+C2H4                             6.60E+05    2.5     6763.9
58. C4H6=>2C2H3                                       1.80E+13    0.0    85126.7
59. C4H6+H=>C2H3+C2H4                                 5.00E+11    0.0        0.0
60. C4H6+H=>H2+C2H2+C2H3                              6.30E+10    0.7     6001.4
61. C4H6+OH=>HCO+H+C3H5                               5.00E+12    0.0        0.0
62. C4H6+CH3=>CH4+C2H2+C2H3                           7.00E+13    0.0    18413.0
63. C4H8+H<=>C3H6+CH3                                 7.23E+12    0.0     1290.6

NOTE:  A units mole-cm-sec-K, E units cal/mole
```

Appendix C. Comparison of Results Obtained from Various Opposed-Flow Diffusion Flame Simulations Produced with the San Diego Mechanism and with A38.09_04

This report summarizes an evaluation of the potential to create skeletal finite-rate chemical kinetics mechanisms for modeling solid-fuel ramjet (SFRJ) combustor dynamics via a homogeneous-reactor-simulation-based implementation of the trial mechanism method. Anticipating that the San Diego (SD) mechanism's validity for SFRJ combustor modeling will be established based on results obtained from experiments in which flames produced by combusting (solid) hydroxyl-terminated polybutadiene and (gaseous) N_2–O_2 mixtures in an opposed-flow burner will be spectroscopically probed, I specified a protocol to produce skeletal mechanisms that would (hopefully) mimic the SD mechanism over the entire parameter space expected to be realized in those experiments. The smallest candidate produced (A38.09_04) was vetted for the application. The evaluation included comparing in their entirety temperature (T) and rate of heat release ($\dot{q}_{mass}$) versus distance plots obtained from SD- and A38.09_04-based solutions to 18 different opposed-flow diffusion flame (OFDF) problems. The set included nine different combinations of pressure (P) and velocity of air at the oxidizer inlet (V_{ox}). For each P-V_{ox} combination, two problems were formulated and solved: one with the temperature at the fuel inlet (T_{fuel}) equal to 500 K and the other with it equal to 650 K. In each case, a search was performed to find a velocity of the gas at the fuel inlet (V_{fuel}) that produced a solution that satisfied Eq. 6. Plots derived from those solutions were compared.

It was observed that many plots produced for different P-V_{ox}-T_{fuel} combinations were qualitatively similar to one another. Therefore, it was not considered necessary to present and discuss all of them in the main body of the report. In particular, plots obtained from solutions to problems with a given P-V_{ox} and with T_{fuel} equal to 650 K were qualitatively similar to those produced when T_{fuel} equaled 500 K. Therefore, only the latter were presented. Figures C-1 through C-4 present plots obtained from solutions to four problems in which T_{fuel} was 500 K. They were not presented in the main body of the report because they were qualitatively similar to at least one that was. Figures C-1 through C-4 also include a plot showing any species in the SD mechanism that was not in A38.09_04 and had a mole fraction that at some point exceeded 0.00001.

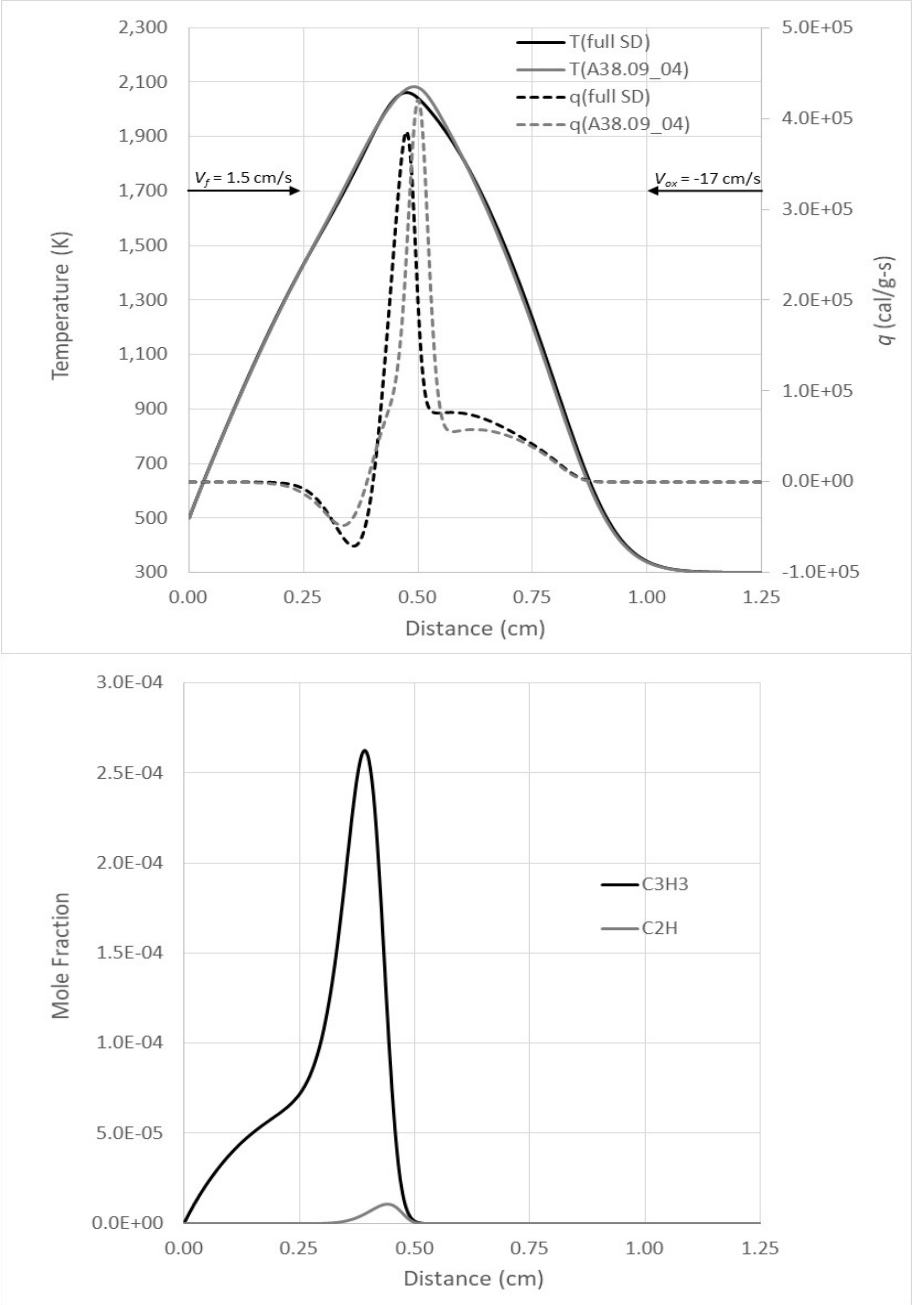

Fig. C-1 Results from OFDF flame simulations with P = 0.4 atm, V_{ox} = 17 cm/s, and T_{fuel} = 500 K. The system's oxidizer-to-fuel ratio (O/F) was 10.1. The lower panel presents results produced with the SD mechanism.

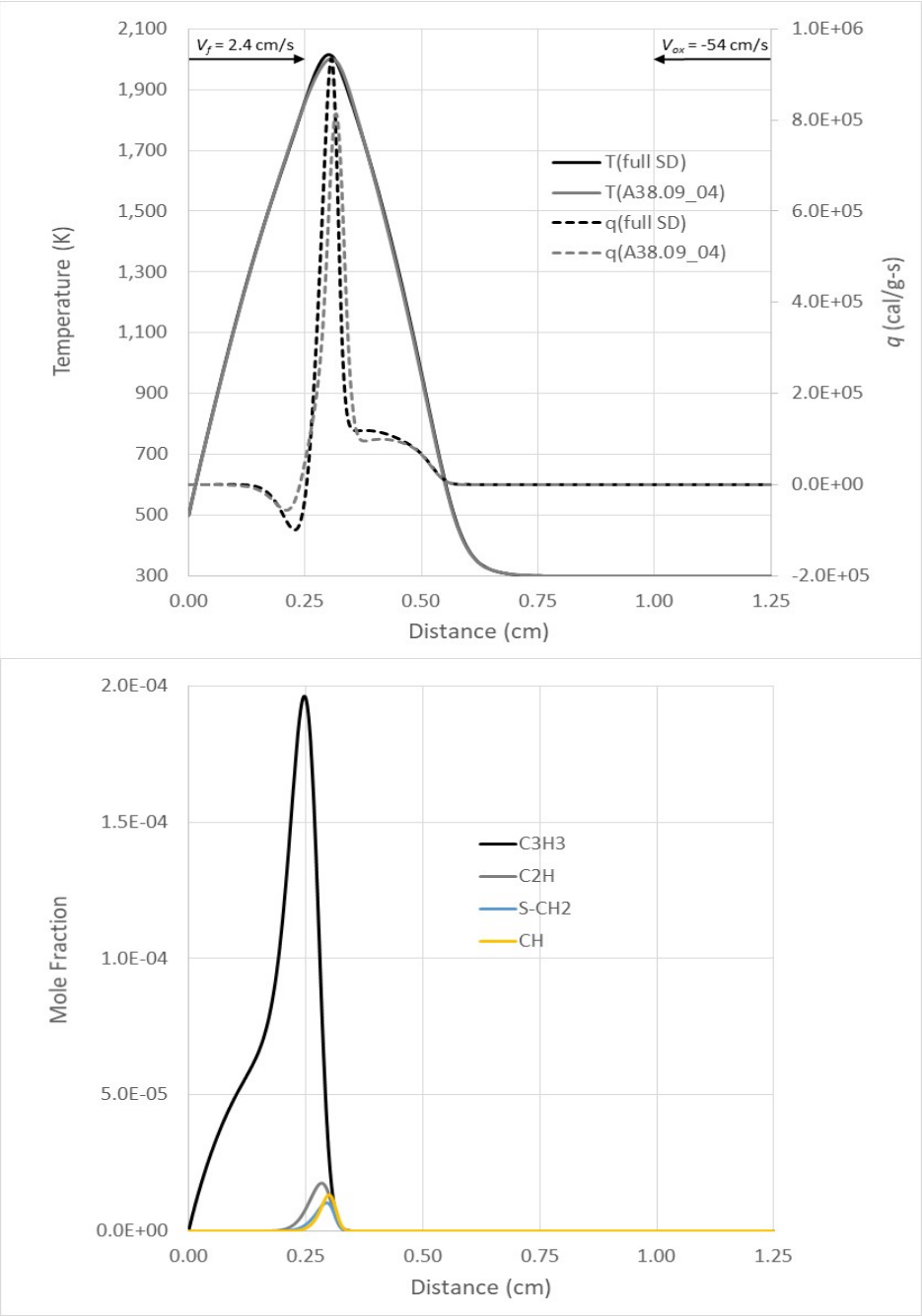

Fig. C-2 Results from OFDF flame simulations with P = 0.4 atm, V_{ox} = 54 cm/s, and T_{fuel} = 500 K. The system's O/F was 20.3. The lower panel presents results produced with the SD mechanism.

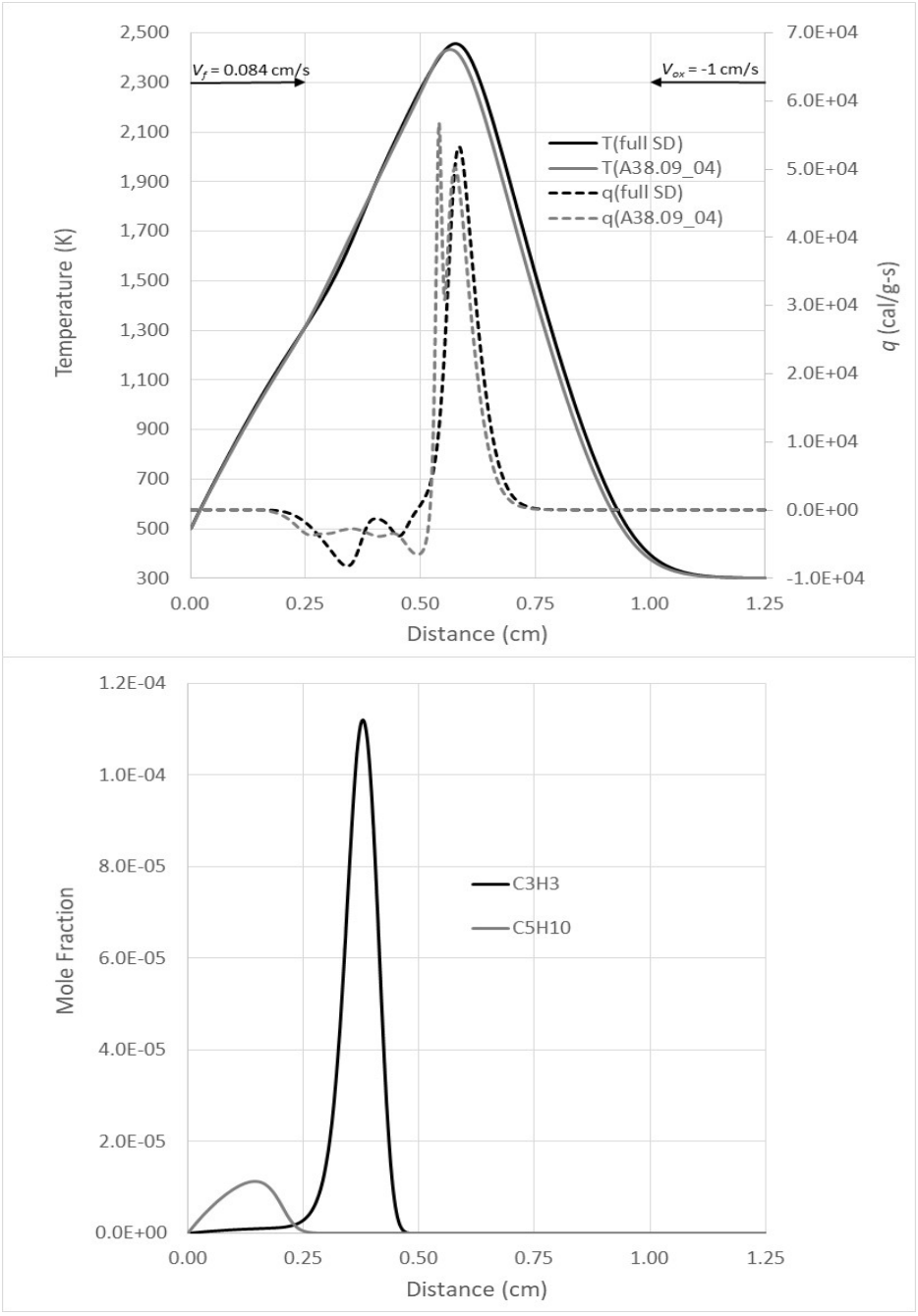

Fig. C-3 Results from OFDF flame simulations with P = 6.2 atm, V_{ox} = 1 cm/s, and T_{fuel} = 500 K. The system's O/F was 10.6. The lower panel presents results produced with the SD mechanism.

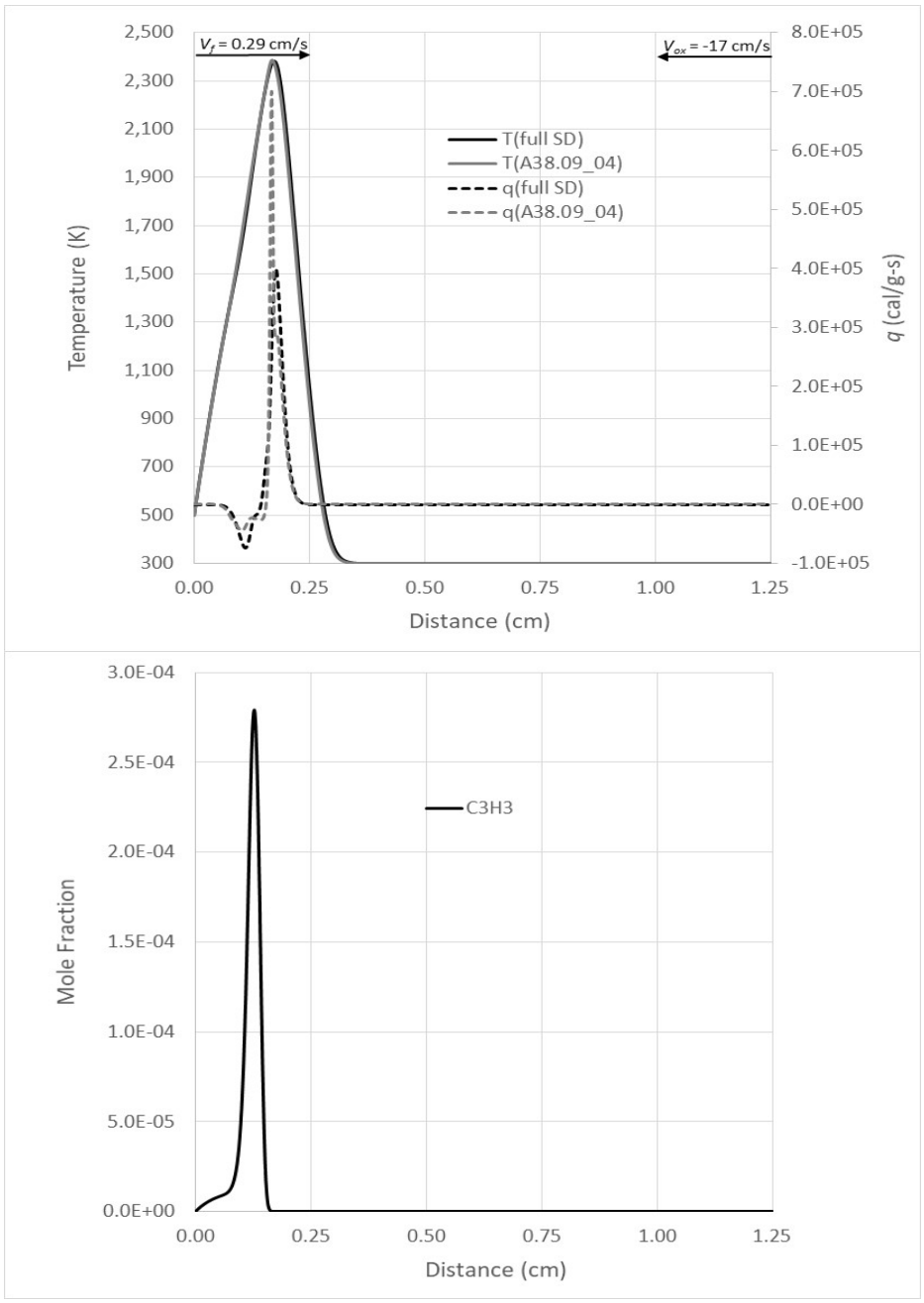

Fig. C-4 Results from OFDF flame simulations with P = 6.2 atm, V_{ox} = 17 cm/s, and T_{fuel} = 500 K. The system's O/F was 63.3. The lower panel presents results produced with the SD mechanism.

List of Symbols, Abbreviations, and Acronyms

1-D	one-dimensional
Ar	argon
ARL	Army Research Laboratory
C_4H_6	1,3-butadiene
CO_2	carbon dioxide
CCDC	US Army Combat Capabilities Development Command
CFD	computational fluid dynamics
H_2O	water
HR	homogeneous reactor
HTPB	hydroxyl-terminated polybutadiene
MADs	maximum acceptable deviations
N	nitrogen
O	oxygen
O/F	oxidizer-to-fuel ratio
OFDF	opposed-flow diffusion flame
SD	San Diego
SFRJ	solid-fuel ramjet
TMM	trial mechanism method

1 (PDF) DEFENSE TECHNICAL INFORMATION CTR DTIC OCA

1 (PDF) CCDC ARL
FCDD RLD CL
TECH LIB

2 (PDF) CCDC AVMC
RDMR WDP P
M PFEIL
RDMR SSM A
M VAUGHN

3 (PDF) NAWCWD-CHINA LAKE
E WASHBURN
B BOJKO
C DENNIS

2 (PDF) NSWC-INDIAN HEAD
H HAYDEN
T HEDMAN

6 (PDF) NRL
B FISHER
R JOHNSON
T LOEGEL
A EPSHTEYN
G GOODWIN
D KESSLER

1 (PDF) ONR
C STOLZ

1 (PDF) AFRL MUNITIONS
S PEIRIS

1 (PDF) USAF
V SANKARAN

18 (PDF) CCDC ARL
FCDD RLR EN
5 (HC) R ANTHENIEN
FCDD RLR PC
J PARKER
FCDD RLV P
L BRAVO ROBLES
FCDD RLW L
T SHEPPARD
FCDD RLW LB
N TRIVEDI
J BRENNAN
E BYRD
FCDD RLW LD
C CHEN
JD VEALS
MJ MCQUAID (1 PDF, 5 HC)
MJ NUSCA
S ISERT
A MCBAIN
A WILLIAMS
J COLBURN
FCDD RLW LH
M MINNICINO
A RAWLETT
J CIEZAK-JENKINS

1 (PDF) EMBRY-RIDDLE AEORNAUTICAL UNIV
S MARTIN

1 (PDF) REACTION SYSTEMS, INC.
B HITCH

3 (PDF) PURDUE UNIV
S SON S
T POURPOINT
C GOLDENSTEIN

1 (PDF) UCSD UNIV
K SESHADRI

1 (PDF) MIT UNIV
W GREEN

1 (PDF) ARGONNE NATL LAB
S KLIPPENSTEIN